

**SORPTION OF SULFONAMIDES BY γ -Fe₂O₃ MODIFIED NATURAL CLAY:
ISOTHERMS, KINETICS AND THERMODYNAMICS STUDIES**

BY

SHIKUKU, VICTOR ODHIAMBO

PHD/SC/00127/2014

**A THESIS SUBMITTED IN PARTIAL FULFILLMENT OF THE REQUIREMENTS FOR
THE DEGREE OF DOCTORATE OF PHILOSOPHY IN CHEMISTRY**

**DEPARTMENT OF CHEMISTRY
SCHOOL OF PHYSICAL AND BIOLOGICAL SCIENCES**

MASENO UNIVERSITY

December, 2018

DECLARATIONS

I declare that this thesis is my original work and has not been previously presented for a degree award in either Maseno University or any other University.

Sign:

Date:

Victor O. Shikuku

Reg No: PHD/SC/00127/2014

Supervisor (s):

This thesis has been submitted for examination with my approval as the University supervisor.

Supervisors:

Prof. Chrispin Kowenje
Department of Chemistry
Maseno University

Signature...



Date...3/12/2018

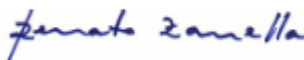
Dr. Fredrick O. Kengara
Department of Chemistry
Maseno University

Signature.....

Date.....

Prof. Dr. Renato Zanella
Laboratory of Pesticides Residues Analysis (LARP)
Federal University of Santa Maria (UFSM), Brazil

Signature



Date:..3/12/2018

ACKNOWLEDGEMENT

First I would like to express my sincere thanks to my first supervisor Prof. C.O. Kowenje for his guidance, motivation and endless support throughout the period of this work. I am grateful for his valuable criticism and encouragement in every step of this study. Thanks to Dr. Keng'ara for his valuable support as well.

I give special thanks to Prof. Dr. Renato Zanella and Prof. D.P Osmar of Laboratory of Pesticide Residue Analysis (LARP), Chemistry department, Federal University of Santa Maria University-Brazil, for their support in facilitating the experimental aspects of this work. I appreciate their expertise and invaluable friendship built during the study period. I wish to extend my sincere gratitude to Dr. Filipe Donato, Nelson Bandeira and all the laboratory staff and students at LARP for their individual and collective support during my research stay.

I acknowledge and appreciate the EXCEED-SWINDON partnership for the PhD research visit scholarship award that facilitated the completion of this work. I also acknowledge the National Research Fund (NRF) for the PhD research grant that aided in the preparation and completion of this work.

I would like to thank Chemistry Department, Maseno University for providing support for this project by facilitating the research collaboration between the two institutions involved. Special thanks go to my family for their endless support, continued patience and love throughout the course of my studies. Finally, and most of all, I thank God Almighty for providence of good health throughout the period of my studies.

DEDICATION

To my mother, 'Judith Opiyo'.

Thank you.

ABSTRACT

In recent years, research has indicated the presence of pharmaceutically active ingredients (PAIs) as emerging water contaminants. The presence of these compounds in surface waters is of great environmental concern due to the toxicological effects of these compounds on organisms in the aquatic environment. Conventional wastewater treatment approaches have been shown to be ineffective in eliminating PAIs from influent wastewater. Among the ecotoxicological PAIs detected in effluents from a typical Kenyan municipal wastewater treatment plant (WWTP) in Bungoma include sulfonamides such as sulfachloropyridazine (SCP) and sulfadimethoxine (SDM). Furthermore, recovery of suspended adsorbent in a continuous flowing system still remains an unresolved challenge. There is therefore an urgent need to investigate and evaluate efficient and cost-effective wastewater treatment alternatives. Iron modified adsorbents have been demonstrated to be economical and efficient adsorbents for removal of various pollutants with adsorbent recovery achievable through external magnetic field. Iron-oxide modified clays, therefore, present a potentially efficient and sustainable alternative due to the natural occurrence and abundance of clay and low cost of iron, hence reduced capital investment. However, the sorption and interaction mechanisms of clays and iron-oxide modified clay for sulfachloropyridazine (SCP) and Sulfadimethoxine (SDM), as model sulfonamides, are not well understood. The objective of this study was to evaluate the sorption characteristics of natural untreated kaolinite clay and iron modified clay (Fe-MC) for SCP and SDM, in single and binary solutions. The effects of initial concentration ($0.25 - 1.25 \text{ mg L}^{-1}$), contact time (15- 360 min) and temperature (303 – 323 K) were investigated. Langmuir model satisfactorily described the sorption of both adsorbates onto the raw and Fe-MC clays. Notably; the raw clay had higher sorption capacity than Fe-MC. In binary solute solutions, an antagonistic sorption process of SDM ($R_{q,SCP} = 0.453$) in the presence of SCP ($R_{q,SDM} = 0.915$) was observed for the raw clay. However, for the Fe-MC clay, an antagonistic sorption process of SCP ($R_{q,SCP} = 0.625$) in the presence of SDM ($R_{q,SDM} = 1.032$) was noted. The antagonisms suggest replacement sorption. For each compound, the sorption reactions obeyed follow a pseudo-second order kinetic law for both clays. However, half-life values depict SDM exhibited faster sorption kinetics over SCP onto the untreated clay while the opposite phenomenon occurred for sorption onto Fe-MC. The calculated thermodynamic parameters, ΔG , ΔH , ΔS and ΔE_a indicate that SCP and SDM sorption on both untreated and Fe-MC clays are spontaneous, exothermic and physical in nature. Intraparticle diffusion model showed that the sorption of the processes followed multiple phases and were not solely controlled by pore diffusion. The proposed sorption mechanisms were found to be consistent with cation bridging and negative charge-assisted H-bonding. The results show the tested clay may be used as a low-cost material for removal of pharmaceutical compounds from wastewater in its raw form.

TABLE OF CONTENTS

DECLARATIONS	I
ACKNOWLEDGEMENT	II
DEDICATION	III
ABSTRACT	IV
ABBREVIATIONS AND ACRONYMS	VIII
LIST OF TABLES	IX
LIST OF FIGURES	X
CHAPTER ONE	2
1.0 INTRODUCTION	2
1.1 Background	2
1.2 Problem Statement	4
1.3 Objectives	4
1.3.1 General Objective	4
1.3.2 Specific Objectives	4
1.4 Null Hypothesis	5
1.4 Null Hypothesis	5
1.5 Justification of the Study	5
CHAPTER TWO	6
2.0 LITERATURE REVIEW	6
2.1 Pollution by Pharmaceutically Active Ingredients	6
2.2 Removal of PAIs from Water	7
2.3 Fundamentals of Magnetic Composites	9
2.4 Natural Sources of Magnetic Minerals	11
2.5 Advantages of Magnetic Composites and Nanocomposites	12
2.6 Iron Modified Adsorbents	13
2.6.1 Adsorption of Heavy Metals Cations	13
2.6.2 Adsorption of Dyes	14
2.6.3 Removal of Organic Micro-Pollutants	17
CHAPTER THREE	19
3.0 METHODOLOGY	19
3.1 Reagents and Instruments	19
3.2 Chromatographic Procedures	19

3.3 Adsorbent Preparation	20
3.4 Adsorbent Characterization.....	20
3.5 Kinetic Studies	21
3.6 Adsorption Isotherm Studies.....	21
3.7 Thermodynamic Studies	22
3.8 Binary Adsorption.....	23
3.9 Data Analysis	24
CHAPTER FOUR.....	25
4.0 RESULTS	25
4.1 Calibration Curves	25
4.2 Adsorbent Characterization.....	25
4.2.1 Chemical Composition	25
4.2.2 Bet Surface Area and Pore Characteristics.....	26
4.2.3 Ftir Analysis	27
4.2.4 X-Ray Diffraction (XRD) Analysis	28
4.3 Adsorption Kinetics	28
4.3.1 Kinetics Studies of SCP and SDM Onto Raw Clay	28
4.3.2 Kinetics Studies of SCP and SDM onto Fe-MC Clay.....	30
4.4 Adsorption Isotherm Studies.....	33
4.4.1 Single Solute Adsorption of SCP and SDM onto Raw (Untreated) Clay	33
4.4.2 Binary Solute Adsorption of SCP and SDM onto Untreated Clay.....	34
4.4.3 Single Solute Adsorption of SCP and SDM onto Fe-MC Clay.....	35
4.4.4 Binary Solute Adsorption of SCP and SDM onto Fe-MC Clay	35
4.5 Thermodynamics of SCP and SDM Adsorption onto Untreated and Fe-MC Clays.....	36
CHAPTER FIVE	38
5.0 DISCUSSION	38
5.1 Adsorbent Characterization.....	38
5.1.1 Chemical Composition.....	38
5.1.2 Textural Characteristics of the Raw and Fe-MC Clays.....	38
5.1.3 Functional Groups Analysis	38
5.1.4 Crystallinity of Raw and Fe-Mc Clays and Structural Changes Analysis.....	39
5.2 Adsorption Kinetics	40
5.2.1 Kinetics Studies of SCP and SDM onto Untreated Clay.....	40

5.2.2 Kinetics Studies of SCP and SDM onto Fe-MC Clay	40
5.3 Adsorption Isotherm Studies	41
5.3.1 Single Solute of SCP and SDM Adsorption onto Raw Clay	41
5.3.2 Binary Solute Adsorption of SCP and SDM onto Untreated Clay	42
5.3.3 Single Solute of SCP and SDM Adsorption onto Fe-MC Clay	43
5.3.4 Binary Solute Adsorption of SCP and SDM onto Fe-MC Clay	44
5.4 Thermodynamics of SCP and SDM Adsorption onto Raw and Fe-MC Clays	46
5.5 Adsorption Mechanism of SCP and SDM onto Raw and Fe-MC Clays	47
5.6 Batch Adsorption Reaction Design	48
CHAPTER SIX	51
CONCLUSION AND RECOMENDATIONS	51
6.1 CONCLUSION	51
6.2 RECOMMENDATIONS	52
6.3 SUGGESTION FOR FURTHER RESEARCH	52
REFERENCES	53

ABBREVIATIONS AND ACRONYMS

pH - Hydrogen ion concentration

BET - Brunauer–Emmett–Teller

XRF - X-ray fluorescence

AAS - Atomic Absorption Spectrophotometry

FTIR - Fourier-transform infrared

SEM - Scanning Electron Microscopy

XRD - X-ray diffraction

pzc - point of zero charge

LIST OF TABLES

Table 1: Some magnetic nanocomposites for heavy metals removal from water.....	14
Table 2: Some magnetic nanocomposites for dye removal from water.....	16
Table 3: The isotherm models.....	22
Table 4: Calibration equations and the correlation coefficients (r^2) for pairs under study.....	25
Table 5: Chemical composition of raw and modified clay	26
Table 6: Adsorbent textural properties.....	26
Table 7: Pseudo-second order kinetic parameters for removal of SCP and SDM onto untreated clay.....	29
Table 8: Pseudo-second order kinetic parameters for removal of SCP and SDM onto CTC	31
Table 9: Calculated adsorption isotherm values for SCP and SDM onto raw (untreated) clay	34
Table 10: Single and binary adsorption of SCP and SDM onto raw clay	34
Table 11: Calculated adsorption isotherm values	35
Table 12: Single and binary adsorption of SCP and SDM onto CTC.....	35
Table 13. Thermodynamic parameters for SCP and SDM adsorption onto raw clay.....	36
Table 14. Thermodynamic parameters for SCP and SDM adsorption onto Fe-MC	37
Table 15: Non-linear regression analysis for SCP and SDM adsorption onto Fe-MC	44

LIST OF FIGURES

Figure 1: Point of zero charge (pH_{pzc}) of Fe-MC.....	27
Figure 2: FT-IR spectrum for the raw and iron modified clay (Fe-MC).....	27
Figure 3: XRD diffractogram for the raw clay and Fe-MC	28
Figure 4: Evolution of adsorption capacity of raw clay for SCP and SDM with time.....	29
Figure 5: Pseudo-second-order kinetic graph for adsorption of SCP and SDM onto raw clay	30
Figure 6: Variation of adsorption capacity for SCP and SDM onto Fe-MC with time.....	31
Figure 7: Pseudo-second-order kinetic graph for adsorption of SCP and SDM onto Fe-MC.....	32
Figure 8: Intra-particle diffusion graph for adsorption of SCP and SDM onto Fe-MC.....	33
Figure 9: Possible adsorption mechanism of SCP on raw clay and Fe-MC	48
Figure 10: Theoretical variation of mass of untreated clay required with volume for SCP and SDM	50
Figure 11: Variation of the theoretical mass of Fe-MC with volume required for SCP and SDM.....	50

CHAPTER ONE

1.0 INTRODUCTION

1.1 Background

Pharmaceutically active ingredients (PAIs) have been shown to be emerging surface water, groundwater and drinking water contaminants raising international concern (Schaidler *et al.*, 2014). These compounds find their way into the aquatic environment through discharge of treated wastewater, seepage from landfills, septic systems and sewer lines and disposal of expired drugs into water systems among other pathways (Glassmeyer *et al.*, 2005). Generally, the concentrations of individual pharmaceutical compounds detected in wastewater treatment effluents are less than 1 $\mu\text{g L}^{-1}$. However, concentrations as high as several mg L^{-1} have been detected in effluent from treatment plants receiving waste from pharmaceutical manufacturing facilities (Phillips *et al.*, 2010). Pharmaceutical compounds have adverse effects, such as disturbance of reproductive and hormone systems, neurobehavioral changes among others, on aquatic organisms even at low concentrations (ng L^{-1}) (Christen *et al.*, 2010). The presence of these compounds in the environment has also been shown to induce development of resistant bacterial strains (Li *et al.*, 2009).

Conventional drinking and wastewater treatment technologies, which largely depend on pollutant adsorption onto activated carbon, are presently known to be ineffective in complete elimination of PAIs from water and the treatment plants have thus become point sources of PAIs loading in surface waters (Daneshvar *et al.*, 2012; K'oreje *et al.*, 2012; Michael *et al.*, 2013). Among the PAIs detected in effluent from a typical Kenyan municipal wastewater treatment plant in Bungoma town include sulfamethoxazole and sulfadoxine representing sulfonamides (Kimosop *et al.*, 2016). Exposure to non-target organisms for sulfonamides has been associated with stomatitis, hemolysis, hepatotoxicity and renal toxicity (Baran *et al.*, 2011; Bialk-Bielinska *et al.*, 2011). Alternative adsorbents are therefore critically needed.

In the face of such challenges, various adsorbents such as water hyacinth derived biochars and zeolites have recently been evaluated for removal of pharmaceuticals ingredients and organic micro-pollutants with commendable results (Ngeno *et al.*, 2016; Shikuku *et al.*, 2015). However, there is still need to evaluate not only cost-effective alternative adsorbents but also with molecular capturing agents for removal of these compounds from wastewater at molecular size limits. In

recent years, nanoparticles pillared adsorbents have been demonstrated as suitable alternative adsorbents for removal of organic pollutants from waters utilizing the synergistic combination of the properties of the guest (nanoparticles) and host molecules (Fakhri and Adami, 2014; Pradeep and Anshup, 2009). However, the nanocomposites, though effective, still suffer the inherent limitation of recovery in a continuous flowing system. Therefore, alternative PAIs sequestration strategies are critically needed with simple and efficient sorbent recovery steps. Consequently, magnetic nanoparticles pillared adsorbents, such as graphene, clays, zeolites etc have been proposed as alternative adsorbents for removal of organic pollutants from water due to their adsorptive properties and fast recovery by magnetic separation (Chang *et al.*, 2015; Attia *et al.*, 2008).

Since antiquity, clays have been used for ceramic materials and water treatment. Of particular interest is application of clays in wastewater treatment due to their abundance in nature, inexpensiveness and eco-friendly properties. In recent years, pillared interlayered clays have received considerable attention in sorption studies of various pollutants (Mehta *et al.*, 2015). Pillarization is expected to increase the materials' porosity, surface area and thermal stability imbuing the composite with higher adsorptive capabilities (Boruah *et al.*, 2015; Tireli *et al.*, 2014).

Iron oxide modified clays have attracted increasing applications due to the low cost of iron and the synergistic combination of the magnetic properties of iron and the adsorptive features of the host material. Furthermore, intercalation of iron particles may increase the interlayer space, which promotes reptation of the molecular adsorbates to the inner active sites within the clay structure (Tireli *et al.*, 2014). However, the characteristics of the intercalated adsorbent and the mechanisms of the adsorbate – adsorbent interactions as affected by time, adsorbate concentration, presence of competing ions and temperature need to be fully understood for possible optimization. These are describable using classical adsorption isotherms and kinetic modeling and associated thermodynamic parameters. Also, the adsorptive features of iron oxide modified clays for removal of sulfonamides from water need to be better understood.

The aim of this study was to fabricate raw clay modified with iron phase. The clay was obtained from Bungoma town (Kenya), near the aforementioned municipal WWTP. The iron modified clay (Fe-MC) was subsequently used for sequestration of two model sulfonamides of varied physicochemical and structural properties, namely, sulfachloropyridazine (SCP) and sulfadimethoxine (SDM), from aqueous media in single and binary solutions.

1.2 Problem statement

The presence of PAIs in the aquatic environment has instigated great concern since these chemicals are known to be toxic to both aquatic organisms and humans. These compounds in the aquatic environment have also been linked to the development of drug resistant bacteria making it difficult to treat certain diseases. Additionally, conventional wastewater treatment plants (WWTP) strategies are insufficient for complete removal of PAIs leading to dispersion of these compounds in the environment through discharged effluents or into the residence water supply systems. Therefore, alternative low cost adsorbents with high affinity for PAIs, faster kinetics, thermodynamically favored sorption processes are critically needed.

1.3 Objectives

1.3.1 General objective

To evaluate the potential of iron-oxide modified natural clay as low-cost adsorbents for removal of sulfonamides compounds from water

1.3.2 Specific objectives

- i. To characterize the natural clay adsorbents before use (surface functional groups, elemental composition, BET surface area, pore volume, clay mineral identity, and pH_{pzc}).
- ii. To synthesize and characterize iron modified clay adsorbent (Fe-MC)
- iii. To determine the effects of contact time, initial PAI concentration, temperature and binary solutions of the pollutants on the sorption of sulfachloropyridazine (SCP) and sulfadimethoxine (SDM) onto the raw and iron modified clay.
- iv. To determine the thermodynamic parameters of the reaction, namely: Enthalpy (ΔH), Gibbs free energy (ΔG), entropy (ΔS) and Arrhenius activation energy (ΔE_a) for the sorption of sulfachloropyridazine (SCP) and sulfadimethoxine (SDM) onto the raw and iron modified clay.
- v. To investigate or infer the sorption mechanism of SCP and SDM onto Fe-MC

1.4 Null Hypothesis

Raw clay modified with magnetic iron-oxide particles does not have remediation potential for removal of sulfonamides from water. The spent adsorbent will not be recoverable by an external magnetic field.

1.5 Justification of the study

Sulfonamides have been repeatedly detected in Kenyan treated wastewaters and in other African water resources indicating their resistance to conventional wastewater treatment technologies as in those in Kenya (K'oreje *et al.*, 2012; Kimosop *et al.*, 2016). Exposure to sulfonamides has been associated with stomatitis, hemolysis, hepatotoxicity and renal toxicity (Baran *et al.*, 2011; Bialk-Bielinska *et al.*, 2011). Therefore, complete elimination of sulfonamides from water resources is of necessity. Most of the reported alternative adsorbents for water purification, though efficient and relatively cost-effective, such as zeolites, clays and biochars, possess the inherent limitation of adsorbent recovery in a continuous flowing system. An efficient adsorbent must therefore possess, among other properties, a simple segregation and adsorbent recovery step from aqueous solution. Incorporation of magnetism by introduction of magnetically responsive elements, such as iron, have been shown not only to potentially increase adsorptive capacity of adsorbents but also improves adsorbent recovery *via* external magnetic field separation (Boruah *et al.*, 2015; Tireli *et al.*, 2014). Since antiquity, clays have been used for water treatment due to their abundance in nature, inexpensiveness and eco-friendly properties. Imbuing the clays with magnetic responsiveness by modification with iron may significantly improve their adsorptive capacity for sulfonamides sequestration and their recovery after use. At the end, an adsorbent system with well understood and optimised kinetics and thermodynamic interactions with PAIs for wastewater treatment will be available.

CHAPTER TWO

2.0 LITERATURE REVIEW

This chapter concisely discusses the occurrence and fate of pharmaceutical compounds in water resources and the adsorption capacities of selected magnetic composite adsorbents under diverse physicochemical conditions for removal of cations, dyes and organic pollutants from wastewater. The sorption mechanisms and performance of selected magnetic composites under different reaction conditions are discussed. Magnetic composites present eco-friendly properties and are demonstrated to be potential alternatives for application in water purification processes subject to commercial viability evaluation before practical use.

2.1 Pollution by pharmaceutically active ingredients

The increasing widespread use of organic compounds and their dispersion through wastewater have resulted in contamination of many ground and surface water systems. Despite the great toxicological environmental impact associated with these compounds, a vast majority of them are not regulated by environmental management organs. These chemicals include poly aromatic hydrocarbons, pesticide, pharmaceuticals, per-fluorinated compounds and flame retardants (Orata *et al.*, 2009; Lisouza *et al.*, 2011; Kim *et al.*, 2013). Though used for beneficial purposes, pharmaceutically active ingredients (PAIs) have been shown to be emerging surface water, groundwater and drinking water contaminants raising international concern (Kolpin *et al.*, 2002; Schaidler *et al.*, 2014). These compounds find their way into the aquatic environment through discharge of treated wastewater, seepage from landfills, septic systems and sewer lines and disposal of expired drugs into water systems among other pathways (Sharma *et al.*, 2006; Kummerer, 2009). Pharmaceutical compounds have adverse effects, such as disturbance of reproductive and hormone systems, neurobehavioral changes among others, on aquatic organisms even at low concentrations (Christen *et al.*, 2010). The presence of these compounds in the environment has also been shown to induce development of resistant bacterial strains and viral resistance (Singer *et al.*, 2007; Straub, 2009; Li *et al.*, 2009a). This calls to question the efficacy of wastewater treatment plants. Generally, removal efficiencies in wastewater treatment plants are dependent on several factors, which include among others; the physico-chemical properties of the compound, method of treatment employed,

climatic conditions, operational conditions of the treatment process and the age of the activated sludge used in the treatment plant (Miège *et al.*, 2009).

Conventional wastewater treatment plants consist of a primary sedimentation process followed by secondary treatment and final sedimentation. Organic pollutants can be transformed from the aqueous phase by hydrolysis, biotransformation or sorption to sludge (Le-Minh *et al.*, 2010). Nevertheless, the removal efficiency may vary based on compound affinity to the aqueous phase (hydrophilicity) or adsorption onto sludge (hydrophobicity). Consequently, utilization of sewage sludge as a fertilizer may lead to dispersion of hydrophobic PAIs into various environmental compartments (Phillips *et al.*, 2010; Daneshvar *et al.*, 2012; Michael *et al.*, 2013) while highly soluble compounds may escape the WWTPs process. Consequently, PAIs have often been detected in treated drinking water (Kim *et al.*, 2007a). Among the PAIs detected in Kenyan treated wastewater effluents include lamivudine, sulfamethoxazole and ibuprofen representing antiretrovirals, antibiotics and analgesics, respectively (K'oreje *et al.*, 2012; Kimosop *et al.*, 2016). These findings succinctly indicate the inefficiency of conventional wastewater treatment technologies and the need for search for alternative strategies.

2.2 Removal of PAIs from water

The occurrence of a large spectrum of PAIs in the environment bespeaks that conventional wastewater treatment plants incompletely remove these compounds (Stackelberg *et al.*, 2004; Al-Rifai *et al.*, 2011). Transformation of PAIs in wastewater treatment plants involves a limited number of biochemical reactions such as hydroxylation, oxidation and de-alkylation resulting into small structural changes of the parent compound (Helbling *et al.*, 2010). Most wastewater treatment plants are designed to reduce effluent nutrient loads, particularly nitrogen and phosphorous, hence preventing eutrophication of recipient waters. Hence, there is need to develop efficient and sustainable strategies to completely remove or significantly reduce the release of PAIs into the environment.

Recently, studies have focused on new, advanced alternative wastewater treatment technologies. For instance, studies show that treatment by ozonation efficiently eliminates a large spectrum of PAIs from water (Hollender *et al.*, 2009; Yang *et al.*, 2011). However, ozonation results in formation of oxidation products, which are potentially as toxic as the parent molecules (von

Gunten, 2003; Teixeira *et al.*, 2011). The use of biofilms for degrading PAIs from aqueous systems has also been reported. For example, *Trichosporon asahii* yeast isolated from caffeine contaminated soil was used to remove caffeine from industrial wastewater (Lakshmi and Das, 2013). Other treatment techniques, which include advanced oxidation processes (AOPs), membrane bioreactors, photocatalysis and electrochemical methods, have also been shown to eliminate various PAIs from water (Basile *et al.*, 2011; Oller *et al.*, 2011). Similarly, these treatment techniques may result in formation of equally toxic by-products during disinfection of drinking water (Yang *et al.*, 2011). Moreover, most of the studies reported have only been evaluated under controlled laboratory conditions and therefore facing a lot of inherent technical difficulties in application to full scale water treatment.

Methods such as AOPs and electrochemical degradation are also expensive compared to existing treatment technologies, at least at the current state of knowledge and technology. However, this technical limitation may change in the future. Other attempts to minimize PAIs loading from hospitals include on-site separation and treatment of urine with high loads of pharmaceuticals (Beier *et al.*, 2011). However, this approach has been linked with high costs and lacking in practicability. The use of adsorption onto a suitable material seems not only to be inescapable but also technically feasible.

Adsorption still remains the most promising cleanup technology that continues to attract interest worldwide (Ruiz *et al.*, 2010). A study by Genc and Dogan (2015) reported adsorption of ciprofloxacin antibiotic onto bentonite, zeolite and pumice. In a separate study, biomass wastes based adsorbents such as water hyacinth biochar have been demonstrated to be efficient low cost adsorbents for removal of ciprofloxacin and caffeine from water (Ng'eno *et al.*, 2016). A study by Mestre *et al.* (2011) reported adsorption of paracetamol and ibuprofen onto activated carbon derived from sisal waste. Braschi *et al.* (2010) successfully eliminated sulfonamides from water using organophilic zeolite Y as adsorbent. These studies point out that naturally occurring material are the most preferred as precursors for development of alternative adsorbents for PAIs removal from water, possibly because of low capital investment required. However, the reported adsorbents and their nanocomposites, though effective, still suffer the inherent limitation of recovery after use in a continuous flowing system (Chang *et al.*, 2015; Attia *et al.*, 2008). Therefore, though the future seems to favor the use of naturally occurring adsorbents, alternative PAIs sequestration

strategies are still critically needed with simple and efficient sorbent recovery steps. To address the challenges, iron oxide pillared adsorbents, such as graphene, clays, zeolites etc are therefore proposed as alternative adsorbents for removal of organic pollutants from water due to their adsorptive properties and possible recovery by magnetic separation. For this study, clay material is selected.

2.3 Fundamentals of magnetic composites

Magnetic effects arise from movements of particles such as electrons, holes, protons, positive or negative ions, which possess both mass and electric charges. A spinning electrically charged particle generates a magnetic dipole, known as *magneton*. A magnetic domain therefore designates a volume of ferromagnetic material in which all magnetons are aligned in the same direction by the exchange forces. This concept of magnetic moment (μ) orientation in response to an external magnetic field is the basis for classification of the different forms of magnetism, namely, diamagnetism, paramagnetism, ferromagnetism, antiferromagnetism and ferrimagnetisms (Akbazadeh *et al.*, 2012).

When an external magnetic field is applied, atomic size current loops are created resulting from the orbital oscillation of the electrons in opposition to the applied field. This weak repulsion is known as *diamagnetism* and is exhibited in all materials. However, due to the weak nature of diamagnetism, any other type of magnetic characteristics inherent in the material normally quenches these current loops. From the electronic configuration perspective, diamagnetism is observed in materials with completely filled electronic subshells such that the magnetic moments are paired and the effective moment is zero since they cancel each other. Diamagnetic materials have a negative susceptibility ($\chi < 0$). On the other hand, all other magnetic properties are associated with unpaired electrons in the subatomic orbitals more often the *3d* and *4f* orbitals (Coey, 2009).

Ferromagnetic materials, such as Fe, Ni and Co, have aligned atomic magnetic moments of equivalent magnitude, and their crystalline structures permit direct coupling interactions between the moments. Additionally, the aligned moments can induce spontaneous magnetization in the absence of an applied external magnetic field. Materials that retain permanent magnetization in the absence of an external field are called hard magnets. Materials possessing atomic magnetic

moments of equivalent magnitude arrayed in an antiparallel pattern, resulting to zero net magnetization, are known as *antiferromagnetic* materials.

Above the magnetic ordering temperature (T_N) also called Néel temperature-named after the French physicist Louis Neel, thermal energy becomes large enough to destroy and randomize the alignment of the equal and oppositely aligned atomic moments in the antiferromagnetic material. The material therefore displays paramagnetic behavior. If the atomic magnetic moments, below the Neel's temperature and in the absence of external field, assume an ordered but unparallel arrangement, the material is said to possess *ferromagnetic* behavior (e.g. magnetite, Fe_3O_4). Normally, within the magnetic domain, significant net magnetization emanates from the antiparallel alignment of adjacent non-equivalent sub-lattices. The resultant macroscopic characteristics are comparable to ferromagnetism. However, above the Néel temperature, the material remodels to *paramagnetism* (Akbazadeh *et al.*, 2012; Coey, 2009).

Reducing the physical size of materials to the nanoscale often result to properties profoundly divergent from their bulk scale (micro/macro) equivalents, such as inner structure, intrinsic electronic and optical properties including magnetic characteristics (Xiaolei *et al.*, 2013). This is particularly important in the technological application of magnetic nanoparticles and their nanocomposites because these differences include departure from the established laws of magnetic behavior of macroscopic materials. Magnetic nanocomposites are therefore composed of ferromagnetic nano-sized particles dispersed either in an amorphous non-magnetic or magnetically soft matrix. The shape, size and distribution of the magnetic particles also significantly affect the properties of the composites.

In order to fabricate a nanomagnetic composite of desired physico-chemical properties, an understanding of the structure of the host materials and their tunability is critical (Singh *et al.*, 2011). This is because the integrity of the synthesized composite for water purification will depend on the structural and textural properties of the matrix, which are a function of the interaction mechanisms of the guest particle surfaces, and the parent matrix. The interaction mechanisms may be through ionic bonds, covalent bonds, van der Waals forces and hydrogen bonding. The better the interaction and dispersion of the nanoparticles on the matrix, the better the overall properties. In general, the macroscopic properties of the magnetic nanocomposites are determined by several factors including the composition of the matrix, the physicochemical properties of each constituent,

the geometry and dispersion of the magnetic particles on the matrix network, guest-guest and guest-host molecular interactions and subsequent modifications of the matrix. It is self-evident that these parameters are closely interlinked. The present study proposes to synthesize and characterize iron oxide-clay composite and evaluate its applicability in water purification.

2.4 Natural sources of magnetic minerals

There is a wide range of exceptionally selective naturally occurring magnetic nanomaterials. Magnetite, a ferromagnetic member of the spinel group of minerals, is the most abundant naturally occurring magnetic mineral, often found in large quantities in beach iron sands. It frequently occurs as a constituent of igneous and metamorphic rocks. Magnetites are also formed by serpentinization of peridotite (or dunite) and as the major product of rusting steel surfaces. Massive deposits of magnetite are spread worldwide including places such as Atacama region of Chile, west coast of the North Island of New Zealand and the Valentines region of Uruguay (Tania, 2012). Other related magnetic minerals that occur in nature are maghemite ($\gamma\text{-Fe}_2\text{O}_3$) and hematite ($\alpha\text{-Fe}_2\text{O}_3$). Under thermal treatment, magnetite can be converted to maghemite and hematite. Another naturally occurring magnetic nanoparticle is the zero valent iron (ZVI). Zero valent iron based nanocomposites have been used extensively in recent times in water purification regimes. Here, the magnetic nanoparticles are either used directly as adsorbents or as the core material in a core-shell nanoparticle structure where the mixed iron oxide shell provides adsorption sites while the magnetic core realizes magnetic segregation (Shengsen *et al.*, 2016). However, for practical purposes, it is worthwhile to note that nanoscale zero valent iron (nZVI) is more reactive than ZVI, and tends to aggregate due to its high surface energy and strong magnetic attraction, which reduces its effective surface area and contact area for targeted pollutants. A possible mitigation strategy to stabilize nZVI is by immobilizing the nZVI particles onto a supporting material such that the properties of both support materials and nZVI are conserved (Yan *et al.*, 2013).

Profiling of the natural abundance of the various forms of iron oxide in various naturally occurring minerals, such as zeolites, clays, sands in Kenya is still limited. In this work, the adsorptive and textural effects of iron oxide on Kenyan clay were explored in possible application to increase adsorption capacities of clay for sulfonamide antibiotics.

2.5 Advantages of magnetic composites and nanocomposites

Magnetic nanocomposites possess the inherent advantages of employing nanoscale particles, that is, high adsorption competence. For example, Yean *et al.* (2005) observed that decreasing the particle size of nano-magnetite from 300 to 11 nm, its adsorption capacity for arsenic increased 100 fold. This is called the “nanoscale effect” attributed to the change of magnetite surface structure; which both increased the specific surface area and created new adsorption sites. Furthermore, as the particle sizes are decreased further, magnetic particles (e.g nano-maghemite and nano-magnetite) become superparamagnetic, losing permanent magnetic moments while responding to an external magnetic field, thereby allowing untroublesome partitioning and recovery by a low-gradient magnetic field. Therefore, the use of magnetically modified adsorbents makes it possible to perform the separation process directly in crude samples containing suspended solid materials by applying an external magnet without necessity of filtration, making the segregation step easier, rapid and effective. Fast mass transfer is thus achievable due to a large contact surface area between the adsorbents and pollutants, facilitating fast kinetics and rapid adsorption equilibrium. This is also attributed to larger specific surface area, large number of active binding sites (edges, vacancies) and short intraparticle diffusion length typical of a nanomaterial.

Magnetite (Fe_3O_4) has been especially widely used as magnetic material due to its excellent magnetic properties, chemical stability and biocompatibility (Kara *et al.*, 2015). Depending on the properties of the carrier material; the synergistic combination of these materials with magnetic particles offers the composite adsorbent distinguished properties such as good dispersity, large surface area, nontoxicity, strong superparamagnetism and excellent extractionability. Therefore, manipulation of magnetic adsorbents is much easier in complex multiphase systems with an external magnetic field. Furthermore, these metal oxides based nanocomposites are easily regenerated by modifying the solution pH (Sharma *et al.*, 2009).

Generally, in most cases, the adsorption capacity of nanocomposite remains robust after 3-10 adsorption-desorption cycles (Chang *et al.*, 2016). Moreover, the temperatures required for reclamation of magnetic nanocomposites are very low, the energy consumption for regeneration is greater than 50% of other strategies, low operating pressures are needed with low-pressure drops, and the performance has high flexibility and stamina. The process also exhibits fast adsorption

kinetics and does not produce contamination and the adsorbents can be fully recovered with minimum or no damage. However, reduction in adsorption capacity after recycling has also been reported (Mayo *et al.*, 2007). Nevertheless, these advantages prevail over the difficulties normally associated with other powdered adsorbents including non-magnetic nanomaterials.

Magnetic composites and nanocomposites are therefore economically and technologically expedient. Like other adsorbents, the nanocomposites can also be functionalized for target molecules. Despite these results, studies on naturally occurring and abundant carriers, such as clay, for these magnetic particles to solve the problem at hand, sequestration of sulfonamides from water, are not only limited but the chemistry is not well understood. The synergistic combination of clay and magnetically responsive oxides and the interactions with sulfonamides has not been documented. This work reports the selective and adsorption capacities of iron oxide modified clay for sulfonamides and proposes possible interaction mechanisms.

2.6 Iron modified adsorbents

2.6.1 Adsorption of heavy metals cations

Conventional water treatment protocols are generally based on powdered activated carbons (PAC) as adsorbents. However, Faulconer *et al.* (2012) demonstrated that magnetite coated PACs have the capacity to sorb up to 84% of Hg (II) ions from solution at 100 µg/L metal ion solution. Similar results were obtained using magnetic iron oxide nanoparticles mutated with 2-mercaptobenzothiazole within a wide range of pH (Parham *et al.*, 2012). The hybrid posted stupendous results of complete removal of 200 µg/L of Hg (II) within 4 minutes of contact time. Short residence times are suitable and economical for water purification systems. Noteworthy, the overall performance of the nanocomposite is dependent on the properties of the nanoparticles host material. As Girginova *et al.* (2010) reported, silica coated magnetite particles ($\text{Fe}_3\text{O}_4/\text{SiO}_2$) have significantly lower magnetic saturation value compared to pure Fe_3O_4 . This is attributed to the fact that the silica shells surrounding the magnetite particles obstruct the interaction between magnetic cores. Consequently, modification of the composite surface by dithiocarbamate groups surface ($\text{Fe}_3\text{O}_4/\text{SiO}_2/\text{NH}/\text{CS}_2^-$) resulted to increased affinity for Hg (II), from 24% to 74%. Careful choice

of the operation pH is critical because of variation of the zeta potential (from negative to positive) of the nanoparticle-mercury complex with pH and Hg (II) concentration.

Table 1: Some magnetic nanocomposites for heavy metals removal from water

Adsorbent	Adsorbate	Adsorption capacity	pH	Temp °C	Ref
Magnetic powdered activated carbon	Hg(II)	91%	4.5	30	(Faulconer <i>et al.</i> 2012)
EDTA functionalized magnetite	Cu(II)	46.27 mg/g	6	25	(Liu <i>et al.</i> 2013)
Magnetic modified sugarcane bagasse	Cd(II)	1mmol/g	5	25	(Yu <i>et al.</i> 2013)
Magnetic graphene/iron oxides nanocomposite	U(VI)	69.49 mg/g	5.5	25	(Zong <i>et al.</i> 2013)

The adsorption mechanisms are elucidated by varying of solution pH and subsequent characterization of the matrix-metal ion complexes employing tools as FTIR and XRD analysis. For instance, most researchers propose that the adsorption mechanism of Co(II) on hydrous ferric oxide to be *via* the reaction with hydroxyl groups, spontaneous precipitation of Co(OH)₂, occupation in the vacancy of iron oxide, or reduction by zero valent iron (Xing *et al.*, 2016). The adsorption mechanisms and extent are thus dependent on host material and cannot be determined *a priori*. Since, clay properties vary widely; empirical data is needed to support the assumed suitability of the proposed adsorbent, iron oxide modified raw clay, for sulfonamide adsorption.

2.6.2 Adsorption of dyes

Dyes and pigments are coloring agents used for value addition in textile and printing among other finished products. The dyes containing effluents from these industries ultimately end into the municipal wastewaters. Besides coloration and making the water odious, dyes are known to possess carcinogenic and mutagenic effects, even at low concentrations. Therefore, environmentally, their elimination from water is of utmost importance.

Chang *et al.* (2016) synthesized Fe₃O₄/activated montmorillonite (Fe₃O₄/Mt) nanocomposite for removal of cationic methylene blue (MB) dye from aqueous media. Incorporation of Fe₃O₄

increased the total pore volume and average pore size in the $\text{Fe}_3\text{O}_4/\text{Mt}$ nanocomposite which was beneficial for adsorption efficacy. Impregnation with iron particles is also known to potentially increase the basal spacing that enhances intercalation of adsorbing molecules. Adsorption was mainly attributed to coulombic interactions between the negatively charged adsorbent surface and the cationic dye as evidenced by the high extraction efficiency over a wide range of pH. However, at lower pH competition between the dye cations and H^+ for the active binding sites becomes significant impeding effective removal efficiency. In such situations, pH values greater than the isoelectric point (pH_{pzc}) of the adsorbent (7.56 in the case of $\text{Fe}_3\text{O}_4/\text{Mt}$) are recommended. Dynamic equilibrium was achieved in 30 min which is suitable for system design with 99% dye removal efficiency. Furthermore, the nanocomposite maintained removal efficiency greater than 83% after 5 cycles with concomitant good magnetic separation effects in an external magnetic field, a testament that $\text{Fe}_3\text{O}_4/\text{Mt}$ is plausibly stable and recyclable.

In another study, Zhang and co-workers (2007) fabricated copper ferrite/activated carbon ($\text{CuFe}_2\text{O}_4@\text{C}$) nanocomposite of different $\text{CuFe}_2\text{O}_4:\text{C}$ ratios by mass for removal of Acid Orange 7. Saturation magnetization was lower, as expected, for the hybrid with less CuFe_2O_4 content. From the isothermal data, it was conceived that the copper ferrite particles homogenized the surface of activated carbon though it was the activated carbon in the matrix that was predominantly responsible for the adsorbed dye. Therefore, the dual function of the magnetic nanoparticles was surface tuning and for easing adsorbent recovery.

In a separate study, Zhang and Kong (2011) produced magnetic $\text{Fe}_3\text{O}_4/\text{C}$ core-shell nanoparticles of 250 nm average size for sequestration of two organic dyes, namely methylene blue and cresol red from water. Magnetic susceptibility investigations showed the composite to be superparamagnetic. The adsorption capacities for methylene blue (MB) and cresol red were 44.38 mg/g and 11.22 mg/g, respectively within the experimental conditions. The higher affinity for MB was attributable to the hydroxyl and carbonyl functional groups on the surface of the composite and the negative potential of the magnetic nanoparticles creating weak coulombic interaction between the cationic dye and the adsorbent. A list of available magnetic sorbents, optimal reaction conditions and adsorption capacities for other dyes are listed in Table 2.

Table 2: Some magnetic nanocomposites for dye removal from water

Adsorbent	Adsorbate	Adsorption capacity (mg/g)	pH	Temp.	Ref
Magnetic carbon-iron oxide nanocomposite	Crystal violet	111.8	8.5	50	(Singh et al. 2011)
Magnetic Fe ₃ O ₄ @ grapheme	Congo red	33.06	n.p	n.p	(Yao et al. 2012)
Superpara-magnetic rectorite nanocomposite	Neutral red	16.0	n.p	n.p	(Wu et al. 2011)
Magnetic N-lauryl chitosan nanocomposite	Remazol red 198	267	n.p	n.p	(Debrassi et al. 2012b)
Magnetic zeolite/iron oxide nanocomposite	Reactive Orange	16 1.1	n.p	25 ± 2	(Fungaro et al. 2011)
Graphene-Fe ₃ O ₄ nanocomposite	Pararosaniline	198.23	3–5	25	(Wu et al. 2013)
Magnetic ferrite nanoparticle alginate composite	Basic Blue 9	106	8	-	(Mahmoodi, 2013)

n.p- not reported

The results depict that for the same magnetic adsorbent, the adsorption behavior varied significantly for different dyes and therefore the adsorbate properties alone determine adsorption efficiency under similar reaction conditions. The above results, though including iron-oxide modified clays, cannot therefore accurately predict the sorption patterns of the clays for sulfonamides. Experimental evidence from the above suggested interaction parameters are thus still required.

2.6.3 Removal of organic micro-pollutants

The presence of pharmaceutically active ingredients (PAIs) in water resources has not only raised international environmental concern but has also sparked research on techniques for removal of these compounds from water (Ngumba *et al.*, 2016).

Peng *et al.* (2014) synthesized magnetically impregnated montmorillonite as an adsorbent for the elimination of humic acid from water. A removal efficiency of 96% was reported at pH 6.1. Noteworthy, the adsorption was strongly dependent on pH and ionic strength. The authors realized ligand exchange reaction between -COOH groups of humic acid and the montmorillonite as the adsorption mechanism. The extraction efficiency increased with increase in ionic strength. This phenomenon is a consequence of the compression of the diffuse double layer and the molecular volume of humic acid and charge neutralization.

Carbon nanotubes (CNTs) are also facile matrices for fixation of magnetic nanoparticles. An adsorption study demonstrated that CNTs/Fe₃O₄ nanocomposites have the capacity to remove Bisphenol A (BPA) from wastewater (Ghosh *et al.*, 2013). Fe₃O₄ has a characteristic absorption band in FTIR spectroscopy centered at 584 cm⁻¹ assigned to the Fe–O–Fe stretching and bending modes and the band is useful in assessing successful incorporation of Fe₃O₄ in the composite. The BET surface area depends on the CNTs:Fe₃O₄ ratio calculated as 17.9 to 50.6 m² g⁻¹ for 10% CNTs/Fe₃O₄ and 50% CNTs/Fe₃O₄, respectively. On the contrary, incorporation of the magnetic magnetite nanoparticles decreases the micropore volume of the CNTs. The magnetic saturation value (*M_s*) for Fe₃O₄ was, as expected, higher than that for CNTs/Fe₃O₄ due to grafting of CNTs onto Fe₃O₄ surface (Ghosh *et al.*, 2013). Furthermore, no significant changes in the coercivity of the central loop of the samples were observed. Such excellent magnetic properties depict a strong magnetic response of CNTs/ Fe₃O₄, which enables the adsorbent to be easily recovered and recycled from aqueous solution in the presence of an external magnetic field. The increase in specific surface area with increase in CNTs content has a positive influence on the adsorption capability for BPA and other adsorbates as well. This depicts that the additive content of CNTs in the nanocomposite plays a significant driving role in the adsorption process. However, the increase in CNT content resulted to a decrease in the magnetic response of the nanocomposite which is unfavorable for separation from aqueous media. 20% CNTs/ Fe₃O₄ sample therefore presents the best ratio with a

suitable net combined effect of a relatively high adsorption potential but also a strong magnetic response. The adsorption process was well described by the Freundlich isotherm model indicating a heterogeneous distribution of the adsorption sites (Ghosh *et al.*, 2013).

Research indicates that new magnetic composites and nanocomposites continue to be developed each day and their suitability for target compounds are commendable. Nevertheless, there are still knowledge gaps upon which future research must focus. Though iron modified clays have been shown to be suitable adsorbents for removal of heavy metals, dyes and some organic pollutants, there is no data on the suitability of iron modified clays for removal of sulfonamides from water. The adsorption extents and mechanisms also vary depending on the type of clay mineral and the nature and physico-chemical properties of the adsorbates. Experimental data is still needed from which behavior of similar class of compounds from the same adsorbent can be determined *a priori*. Such data is lacking for sulfonamides. The objective of this work was to fabricate raw clay modified with iron phase. The iron modified clay (Fe-MC) was then subsequently used for sequestration of sulfonamides of varied physicochemical and structural properties, namely, sulfachloropyridazine (SCP) and sulfadimethoxine (SDM), from aqueous media in single and binary solutions.

CHAPTER THREE

3.0 METHODOLOGY

This chapter outlines the methods used throughout the study. The reagents used, instruments and experimental set-ups are described.

3.1 Reagents and instruments

The standards for sulfachloropyridazine (SCP) and sulfadimethoxine (SDM) were purchased from Dr. Ehrenstorfer, (Germany). HPLC grade solvents, namely, methanol and acetonitrile were supplied by Mallinckrodt, (NJ, USA). Analytical grade sodium hydroxide, hydrochloric acid, iron (III) chloride hexahydrate and iron (II) sulphate heptahydrate were obtained from Kobian Kenya Limited (Nairobi, Kenya).

For instrumentation, water purifier Milli-Q system UV3 Direct (18.2 M Ω cm resistivity) from millipore (Bedford, MA, USA), analytical balance accurate model APX 200 (Denver Instrument, Thorium Unitech, USA), Ultrasound bath Bandelin Sonorex RK 510 (Walldorf, Germany), Vacuum Pump Tecnal TE-058 (Piracicaba, SP, Brazil), Liquid Chromatograph Varian (Palo Alto, CA, USA), equipped with pump model 210, diode array detector (DAD) Pro Star 335, data acquisition system Star Workstation 6.0, analytical column Gemini 5 μ C₁₈ (250 \times 4.6 mm id; 5 μ m) and guard column (20 \times 1 mm) of the same material, both containing octadecylsilane-modified silica (Phenomenex, Torrance, CA, USA), X-ray Brucker diffractometer (D8 Advance) with copper radiation (K_{α} =1.5406), Perkin Elmer (400 FT-IR spectrometer) with ATR (attenuated total reflection) attached and automatic micropipettes with variable capacity (Brand, Germany and Eppendorf, Canada) were used.

3.2 Chromatographic procedures

Sulfachloropyridazine (SCP) and sulfadimethoxine (SDM) concentrations in the solution were determined using HPLC-DAD Varian (Palo Alto, CA, USA) at 270 nm. The mobile phase was a mixture of water (1 % acetic acid) and acetonitrile (90:10 v/v), with a flow rate of 1.0 mL min⁻¹. The injection volume was 50 μ L.

The analytical curve was constructed for each sulfonamide in the concentration range 1-2 mg L⁻¹ prepared in HPLC grade acetonitrile.

3.3 Adsorbent preparation

The raw clay material, obtained from clay deposits in Bungoma town-Kenya ($0^{\circ} 33'48.60''\text{N}$, $34^{\circ} 33'37.98''\text{E}$) at 15-20 cm depth, were crushed and homogenized for the adsorption experiments. The material was then be sieved through 220 μm sieve for uniform particle size. The adsorbent was then washed in millipore water to remove impurities. The final material (grey in color) was thermally dried to constant weight at 333 K with no further chemical modifications. Iron oxide modified clay (Fe-MC) was prepared following the protocol described by Salem *et al.* (2013). Briefly, 0.5 g of homogenized clay was mixed with 6.1 g of $\text{FeCl}_3 \cdot 6\text{H}_2\text{O}$ and 4.2 g of $\text{FeSO}_4 \cdot 7\text{H}_2\text{O}$ and then dissolved in 100 mL of deionized water. The pH of the mixture was then adjusted to 10.0 using 0.1 M NaOH then the matrix sonicated afterwards agitated in a rotary shaker at 160 rpm for 8 h. Thereafter, 25 mL of 6.5 M NaOH was slowly added and mixed for an hour with the above solution. The resulting black precipitate was then washed with millipore water and finally heated in an oven at 373 K for about 18 hours.

3.4 Adsorbent characterization

The specific surface areas of the adsorbents was calculated from the BET liquid nitrogen adsorption-desorption method conducted at 77 K employing a Micromeritics apparatus (Quadratorb Evo 4, Quantachome, USA). The infrared spectrum of the unmodified and modified raw clay adsorbent sample was obtained *via* ATR-FTIR spectrometer (Nicolet iS-5, USA) over the wavenumber range 4000–400 cm^{-1} . The elemental composition was determined by X-ray fluorescence (XRF). The crystalline phases will be determined using X-ray Brucker diffractometer (D8 Advance) with copper radiation ($K_{\alpha} = 1.5406$). The point of zero charge (pH_{pzc}) was determined using the pH drift method (Hosseinzadeh and Mohammadi, 2015). Precisely, 0.3 g of the adsorbent was mixed with 30 mL of deionized water in separate conical flasks at room temperature. The pH of the solutions was adjusted to 2, 4 and 6 using HCl (0.1 mol L^{-1}). This is the initial pH (pH_i). After a contact time of 8h the suspension was filtered then the final pH (pH_f) measured. The experiments were repeated with initial pH adjusted to 8 and 10 using NaOH (0.1 mol L^{-1}). The difference between pH_i and pH_f values ($\Delta\text{pH} = \text{pH}_f - \text{pH}_i$) was then plotted versus the pH_i .

3.5 Kinetic studies

The sorption kinetic experiments were performed by batch mode separately and in triplicate for SCP and SDM PAIs. A mass of 0.1 g of the Fe-MC was dispersed into a 250 mL conical glass flask containing 50 mL of a 2 mg L⁻¹ PAI compound and agitated at 200 rpm using an overhead temperature-controlled shaker for 7 h. At pre-determined regular time intervals (0.25, 0.5, 1, 2, 3, 4, 5, 6), residual SCP and SDM in solution was determined by a HPLC-DAD. The amount of PAI adsorbed per unit mass at specified time (q_t) was obtained by the expression:

$$qt = \frac{(C_o - C_t)V}{M} \quad (1)$$

Where C_o and C_t are the initial and concentration at time t (mg L⁻¹), respectively. M is the mass (g) of the adsorbent and V is the volume of the solution (L). To generate the kinetics parameters, the kinetic data were fitted to the pseudo-first-order and pseudo-second-order equations given below.

$$\text{Pseudo-first-order model: } \log(q_e - q_t) = \log q_e - \frac{k_1}{2.303} t \quad (2)$$

$$\text{Pseudo-second-order model: } \frac{t}{q_t} = \frac{1}{k_2(q_e)^2} + \frac{t}{q_e} \quad (3)$$

Where t (mins) and q_t (mg g⁻¹) are time and amount adsorbed at equilibrium time, respectively while q_e is the equilibrium sorption capacity and k_1 and k_2 are rate constants.

The percent removal (%R) of each PAI was determined using the equation (Shikuku *et al.*, 2015):

$$\% R = \frac{(C_o - C_e)}{C_o} \times 100 \quad (4)$$

3.6 Adsorption Isotherm studies

To obtain the adsorption isotherm, 0.1 g Fe-MC was separately, in triplicate vessels dispersed into 50 mL of SCP and SDM solutions with varying concentrations ranging from 0.25 to 1.25 mg L⁻¹ at 303 K. After equilibration, the solutions were decanted and the supernatant filtered through 0.2 μm

nylon filters, the residual PAI in solution was analyzed and the equilibrium sorption capacity, q_e at different initial adsorbate concentration obtained by the equation (Shikuku *et al.*, 2015):

$$q_e = \frac{(C_o - C_e)V}{M} \quad (5)$$

The experimental data were then fitted to linearized Langmuir and Freundlich isotherm equations shown in Table 3.

Table 3: The Isotherm models

Isotherm Model	Nonlinear form	Linear form	Parameters	Reference
Langmuir	$q_e = Q_o \frac{K_L C_e}{1 + K_L C_e}$	$\frac{1}{q_e} = \frac{1}{Q_o} + \frac{1}{Q_o K_L C_e}$ $R_L = \frac{1}{1 + K_L C_o}$	Q_o (mg/g), K_L (L/g) R_L	Langmuir, 1916 Hall <i>et al.</i> , (1966)
Freundlich	$q_e = K_f C_e^{1/n}$	$\log q_e = \log K_f + \frac{1}{n} \log C_e$	K_f, n	Freundlich, 1906
Temkin	$q_e = B \ln A_T \cdot C_e$	$q_e = B \ln A_T + B \ln C_e$	A_T, B	Temkin, 1941

Where q_e (mg g⁻¹) and C_e (mg L⁻¹) are the solute uptake and the solution concentration at equilibrium, respectively and Q_o (mg g⁻¹) is the monolayer adsorption capacity. C_o (mg L⁻¹) and R_L are the initial solution concentration and Langmuir separation constant, respectively. The K_L (L mg⁻¹) and K_f are the Langmuir and Freundlich constants and $1/n$ is related to the adsorption affinity or surface heterogeneity (Galhetas *et al.*, 2014).

3.7 Thermodynamic studies

The effect of temperature changes on the sorption was studied in the range 303-323 K. Here, 0.1 g of each adsorbent (raw clay and Fe-MC) was separately dispersed into 50 mL of 1 mg L⁻¹ of SCP and SDM and the contents shaken at different temperatures (303, 313 and 323 K), all in triplicate, until equilibration (Shikuku *et al.*, 2015).

The thermodynamic parameters, namely, change in free energy (ΔG), enthalpy (ΔH) and entropy (ΔS), which indicate the practical feasibility of the process, post-adsorption structural changes of the adsorbent and the sorption mechanism, were derived from the van't Hoff equation:

$$\ln K_c = \frac{-\Delta H}{RT} + \frac{S}{R} \quad (6)$$

$$K_c = \frac{q_e}{C_e} \quad (7)$$

$$\Delta G = -RT \ln K_c \quad (8)$$

Where K_c is the distribution coefficient, T is the temperature (in Kelvin) and R is the universal gas constant (8.314 J/mol K).

The sorption activation energy (E_a) and sticking probability (S^*) were computed from experimental data using modified Arrhenius type equation related to surface coverage (θ) by (Mahmoud *et al.*, 2015):

$$S^* = (1-\theta)e^{-E_a/RT} \quad (9)$$

The S^* is dependent on the adsorbate/adsorbent system under study, its value lies in the range $0 < S^* < 1$ and is a function of temperature of the system. The value of θ was calculated from the following relation:

$$\theta = \left[1 - \frac{C_e}{C_0} \right] \quad (10)$$

3.8 Binary adsorption

0.1g of the adsorbent was dispersed into 50 mL binary solution containing 1 mg L⁻¹ SCP and 1 mg L⁻¹ SDM and stirred at 200 rpm at 303 K, also in triplicate. After equilibration, 1.0 mL aliquots were withdrawn from the flask and transferred into sealed glass vials for residual SCP and SDM present in the solution analysis as above.

The effect of the simultaneous presence of the two compounds, on the bi-component extraction efficiency of Fe-MC was evaluated by computing the ratio of the equilibrium sorption capacity (R_q), defined as:

$$R_{q,i} = \frac{q_{b,i}}{q_{s,i}} \quad (11)$$

Where $q_{b,i}$ and $q_{s,i}$ are the equilibrium sorption capacity (q_e) of compound i in the binary solution and in the single component solution, respectively, under similar experimental conditions (Istratie *et al.*, 2016).

3.9 Data analysis

Data analysis was done using linear regression, non-linear regressions and error bars in Microsoft excel program represented in graphical format using Origin 8.0 software.

CHAPTER FOUR

4.0 RESULTS

This chapter describes the results obtained from the various sample treatments from development of calibration curves, adsorbent characterization to sorption kinetics, isotherms and thermodynamics parameters. The physical meaning and interpretations are not herein discussed.

4.1 Calibration Curves

In order to obtain the residual SCP and SDM concentrations, the calibration curves obtained in the concentration range 1-2 mg L⁻¹ afforded a linear regression coefficient, $R^2 > 0.99$ for each pharmaceutical compound. The respective linear equations are listed in Table 4. The control experiments indicated that undetectable amounts of the SCP and SDM were adsorbed on the glass container walls while the pH ranged 6.3-6.5 for all samples following the treatment with clay and hence were considered to be constant. The linearity ensured reliable quantitative analysis.

Table 4: calibration equations and the correlation coefficients (R^2) for PAIs under study

Compound	Equation	R^2
SCP	$y = 653.5x + 305.8$	0.999
SDM	$y = 1286.x + 15036$	0.997

4.2 Adsorbent characterization

4.2.1 Chemical composition

The elemental composition of oxide form of the raw clay (untreated) (RC) and chemically treated clay (Fe-MC) obtained from X-ray fluorescence (XRF) analyses as presented in Table 5 depict successful incorporation of iron in to the clay matrix. The raw clay contained oxides of various cations including Na, K, Mg, Ba, Ca and Zr and the relative variation in their percentages after chemical treatment are shown in Table 5.

Table 5: Chemical composition of raw and modified clay

Major oxides	Clay materials (wt %)	
	Raw clay	Fe-MC
SiO ₂	43.8	44.3
Al ₂ O ₃	16.9	14.3
Na ₂ O	0.62	8.18
Fe ₂ O ₃	6.67	7.71
K ₂ O	1.61	1.22
MgO	0.89	0.89
TiO ₂	0.84	0.58
CaO	0.55	0.53
Cr ₂ O ₃	0.04	0.02
ZrO ₂	0.33	0.30

4.2.2 BET surface area and pore characteristics

The textural characteristics describing the Brunauer–Emmett–Teller (BET) specific surface area and pore volumes of the raw and treated clay samples are listed in Table 6. The points of zero charge (pH_{pzc}) determined by the pH drift method are also presented. Figure 1 shows the plot for the point of zero charge.

Table 6: Adsorbent textural properties

	Raw clay	Iron Modified clay
Pore radius (nm)	3.73	4.26
Pore volume (cm ³ /g)	0.05	0.05
BET surface area (m ² /g)	10.30	10.26
pH_{pzc}	6.1	6.1
Si/Al ratio	2.29	2.77

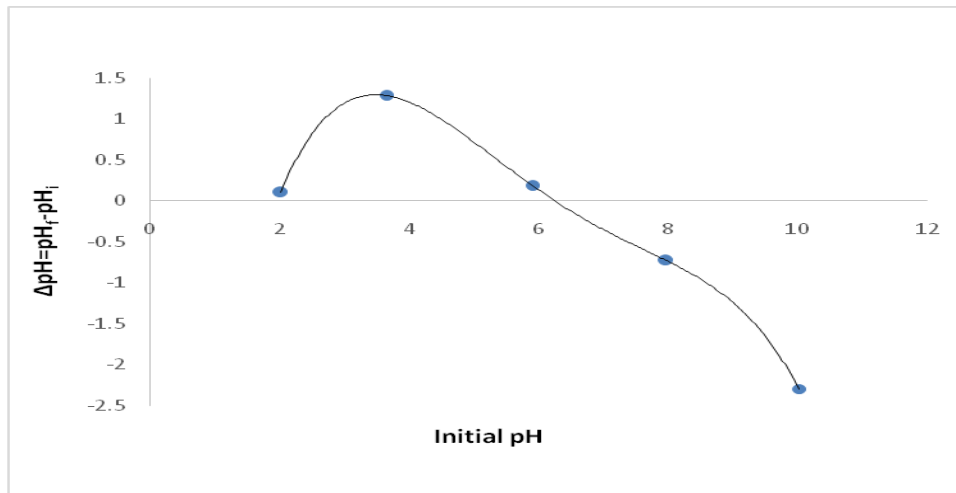


Figure 1: Point of zero charge (pH_{pzc}) of Fe-MC

4.2.3 FTIR analysis

The structural features and functional groups present are displayed in the FTIR plot (Fig. 2). There was observed strong absorption band at 3694 cm⁻¹ and a prominent band at 3619 cm⁻¹. Other significant absorption bands are 910 cm⁻¹ and 1635 cm⁻¹. There was also noted a relative reduction of the 1635 cm⁻¹ peak in Fe-MC. Other two important bands are centered at 595 cm⁻¹ and 684 cm⁻¹ wavenumbers.

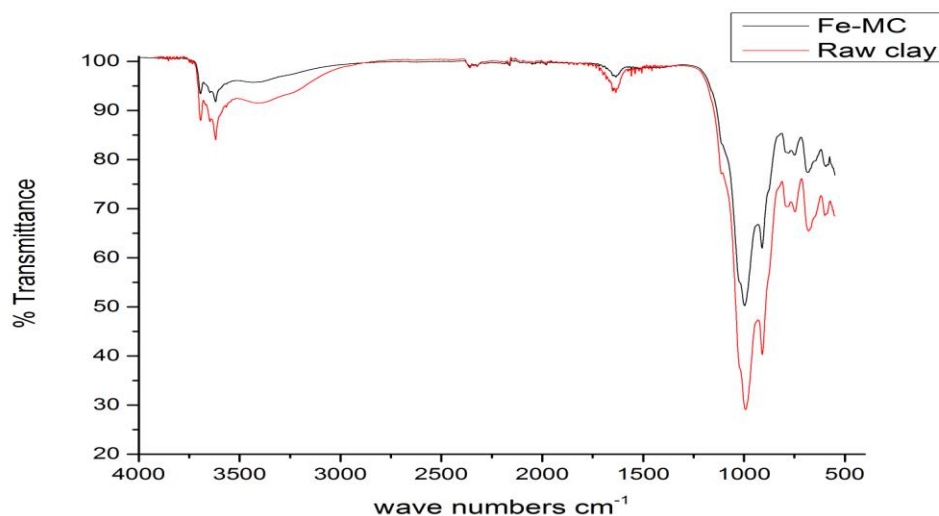


Figure 2: FT-IR spectrum for the raw and iron modified clay (Fe-MC)

4.2.4 X-ray diffraction (XRD) analysis

The XRD patterns of the two samples are displayed Fig. 3. As it can be seen from the diffractogram, there were diminished diffraction peaks at $2\theta = 11.98^\circ$, 20.70° , 21.30° and 45.18° and sharp peaks at $2\theta = 26.48^\circ$, 31.52° and 42.28° . For the Fe-MC there was a slight but noticeable decrease in the intensity of the peak at $2\theta = 26.48^\circ$. The interlayer space was 7.27\AA for both raw and Fe-MC clay samples.

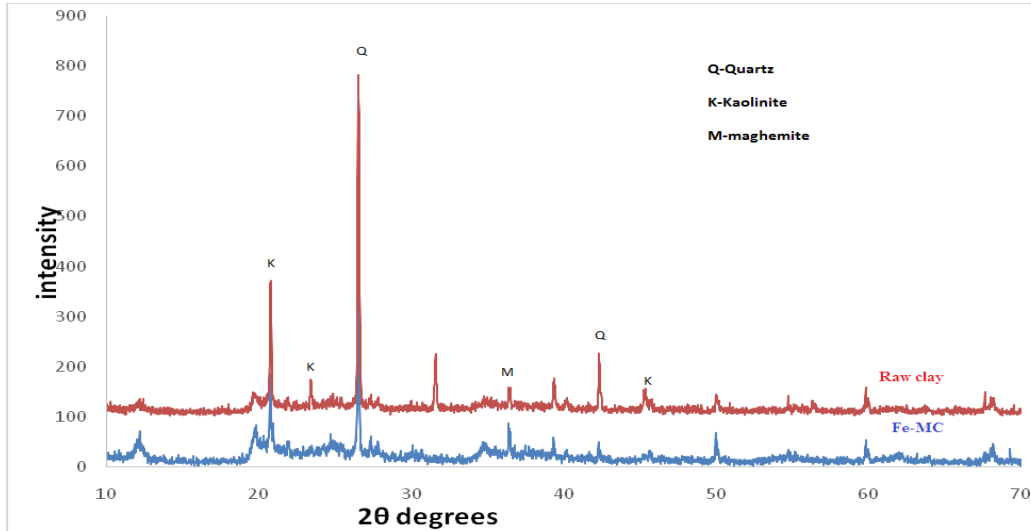


Figure 3: XRD diffractogram for the raw clay and Fe-MC

4.3 Adsorption kinetics

4.3.1 Kinetics studies of SCP and SDM onto raw clay

The time-dependent evolution of untreated clay sorption capacity for SCP and SDM depicted fast sorption kinetics leading to saturation within 180 min (Fig. 4) followed by an equilibrium phase. Noteworthy, the raw clay exhibited higher removal efficiency for SCP (77%) than SDM (50%).

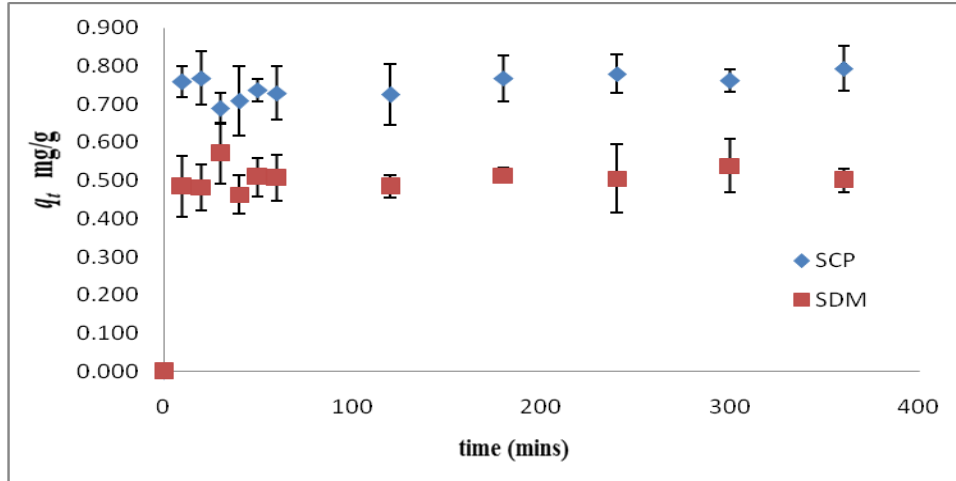


Figure 4: Evolution of sorption capacity of raw clay for SCP and SDM with time ($m= 0.1\text{g}/ 50\text{mL}$, $C_i= 2 \text{ mg L}^{-1}$, $\text{pH}=6.4$)

The sorption dynamics for SCP and SDM onto the raw clay were analyzed using linearized Lagergren pseudo-first order (Equation 2) and pseudo-second order kinetic models (Equation 3). The sorption half lives ($t_{1/2}$) and initial sorption rate (S_{rate}) were derived from the pseudo-second order regression plot using Eq. 12 and 13, respectively (Ho and McKay, 1998) and the computed values are presented in Table 7:

$$t_{1/2} = \frac{1}{k_2 q_e} \quad (12)$$

$$S_{rate} = k_2 q_e^2 \quad (13)$$

Table 7: Pseudo-second order kinetic parameters for removal of SCP and SDM onto raw clay

Compound	$t_{1/2}$ (min)	S_{rate} mg.g/min	k_2 g.mg/min	$q_{e(cal)}$ mg g ⁻¹	$q_{e(exp)}$ mg g ⁻¹	R^2
SCP	3.873	0.204	0.328	0.788	0.776	0.999
SDM	1.179	0.437	1.649	0.514	0.515	0.997

The data poorly fitted the pseudo-first order model with low R^2 values. On the contrast, the the pseudo-second-order kinetics law yielded with R^2 (>0.99) closest to unity (Fig. 5) with close agreement between the calculated (q_{cal}) and experimental (q_{exp}) sorption capacities (Table 7).

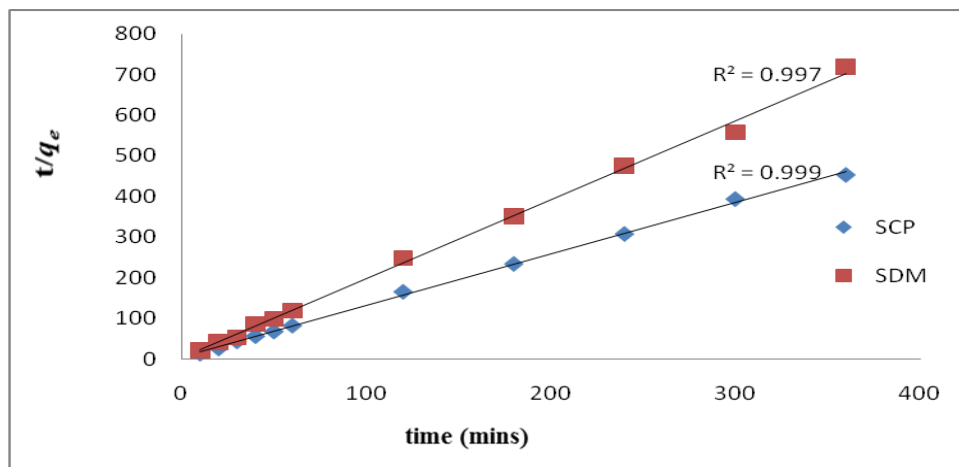


Figure 5: Pseudo-second-order kinetic graph for sorption of SCP and SDM onto raw clay ($m= 0.1$ g/ 50 mL, $C_i= 2$ mg L⁻¹, pH=6.4)

4.3.2 Kinetics studies of SCP and SDM onto Fe-MC clay

The variation of SCP and SDM retention by Fe-MC clay as a function of time depicted that the sorption extent of the compounds increased rapidly to saturation within 120 min (Fig. 6) followed by a stagnated phase with no appreciable change in concentration with time. As in the raw clay, Fe-MC exhibited higher removal efficiency for SCP (75%) than SDM (45%).

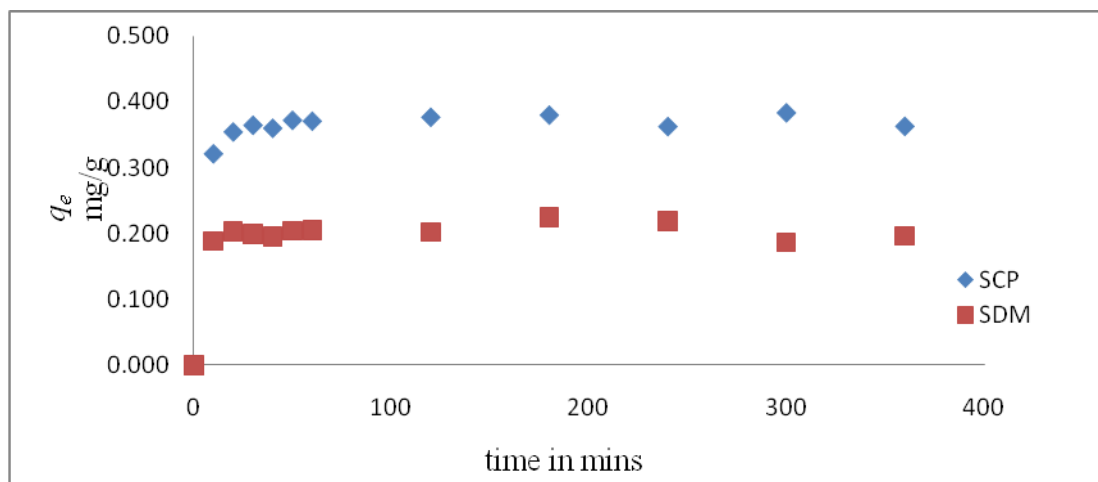


Figure 6: Variation of sorption capacity for SCP and SDM onto Fe-MC with time ($m= 0.1\text{g}/ 50\text{mL}$, $C_i= 1\text{ppm}$, $\text{pH}=6.4$)

The sorption dynamics were also analyzed using linearized pseudo-first order (Ho and McKay, 1998) and pseudo-second order kinetic models (Ho, 2006) and the calculated parameters are listed in Table 8.

Table 8: Pseudo-second order kinetic parameters for removal of SCP and SDM onto Fe-MC

Compound	$t_{1/2}$ (mins)	k_2 ($\text{g mg}^{-1}\text{min}^{-1}$)	$q_{e(cal)}$ (mg g^{-1})	$q_{e(exp)}$ (mg g^{-1})	R^2
SCP	1.186	2.242	0.376	0.373	0.998
SDM	6.637	0.761	0.198	0.202	0.991

The pseudo-first order presented poor R^2 values whereas the pseudo-second-order coefficients of determination (R^2) were closest to unity (Fig. 7) with less than 2% deviation between the calculated (q_{cal}) and experimental (q_{exp}) sorption capacities (Table 8).

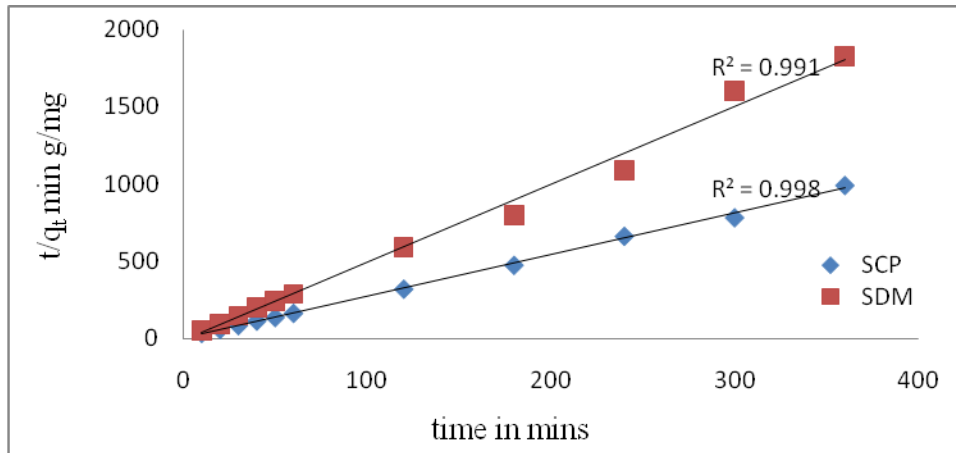


Figure 7: Pseudo-second-order kinetic graph for sorption of SCP and SDM onto Fe-MC ($m= 0.1\text{g}/50\text{mL}$, $C_i= 1\text{ppm}$, $\text{pH}=6.4$)

The kinetic data was also fitted to the intra-particle diffusion model (Equation 14) to predict the rate-controlling step (Weber and Morris, 1963).

$$\text{Intra-particle model: } q_t = k_p t^{0.5} + C \quad (14)$$

where, q_t is the sorption capacity of at a given time t , k_p is the intra-particle rate constant in $\text{mg g}^{-1} \text{min}^{-1/2}$ while C is a constant descriptive of the boundary layer thickness. The regression of q_t as a function of $t^{0.5}$ yielded multi-linear linear plot and did not pass through the origin for both SCP and SDM (Fig. 8).

The intra-particle diffusion model (Equation 14) plot for predicting the rate-controlling step for both SCP and SDM sorption onto Fe-MC is shown in Figure 8. Evidently, the plots were multi-linear and don't pass through the origin.

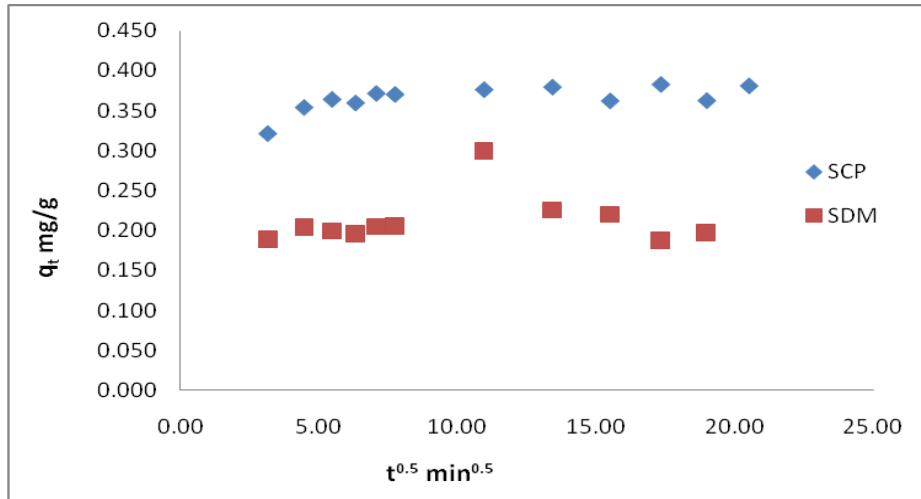


Figure 8: Intra-particle diffusion graph for sorption of SCP and SDM onto Fe-MC ($m= 0.1\text{g}/ 50\text{mL}$, $C_i= 1\text{ppm}$, $\text{pH}=6.4$)

4.4 Adsorption isotherm studies

4.4.1 Single solute sorption of SCP and SDM onto raw (untreated) clay

In the present work, equilibrium data modeling for single component system was done using two linearized isotherms *viz.* Langmuir and Freundlich and their constants are listed in Table 9. The favorability of the sorption process was inspected in terms of the dimensionless separation constant R_L given by equation 14.

$$R_L = \frac{1}{1 + K_L C_o} \quad (15)$$

Where K_L (L/mg) is the Langmuir constant and C_o (mg/L) denotes the adsorbate initial concentration. The calculated R_L values in the present work were in the range $0 < R_L < 1$ (Table 9). The coefficients of determination (R^2) values were fairly high for both Langmuir and Freundlich models. The magnitude of Freundlich constant n , lied between 1-2 for both SCP and SDM while the Langmuir the maximum monolayer sorption density (Q_o , mg g^{-1}) was higher for SCP than SDM onto the untreated clay (Table 9).

Table 9: Calculated adsorption isotherm values for SCP and SDM onto raw (untreated) clay

Isotherm model	SCP	SDM
Freundlich	$R^2=0.96$	$R^2=0.88$
	$n=1.091$	$n=1.283$
	$K_f=1.109 \text{ L mg}^{-1}$	$K_f=0.638 \text{ L mg}^{-1}$
Langmuir	$R^2=0.97$	$R^2=0.86$
	$Q_0=8.547 \text{ mg g}^{-1}$	$Q_0=1.391 \text{ mg g}^{-1}$
	$K_L=0.149 \text{ L mg}^{-1}$	$K_L=0.744 \text{ L mg}^{-1}$
	$R_L=0.770$	$R_L=0.402$

4.4.2 Binary solute sorption of SCP and SDM onto raw clay

The equilibrium experimental data for the simultaneous sorption of SCP onto raw clay in the presence of an equal concentration of SDM (1 mg L^{-1}) is shown in Table 10. Here, the sorption of SDM was significantly abridged by the presence of SCP in the binary system. The equilibrium sorption capacity of SDM decreased from 0.314 mg g^{-1} in the single solute solution to 0.142 mg g^{-1} in the binary solution (Table 10). The value $R_{q,SDM} = 0.453$ is far less than 1. On the other hand, the equilibrium sorption capacity of SCP was 0.353 mg g^{-1} in single solute solution and 0.323 mg g^{-1} in binary solution, resulting to the value $R_{q,SDM} = 0.915$, tending to 1.

Table 10: Single and binary sorption of SCP and SDM onto raw clay

Sorption capacity (mg/g)	SCP	SDM
Single component ($q_{s,i}$)	0.352	0.314
Binary component ($q_{b,i}$)	0.323	0.142

4.4.3 Single solute sorption of SCP and SDM onto Fe-MC clay

In the present work, equilibrium data modeling for single component system onto Fe-MC was done using two widely used two-parameter isotherms *viz.* Langmuir, Freundlich and their constants are listed in Table 11. Sorption of SDM onto Fe-MC showed low linearity posting relatively low coefficients of determination, R^2 , (Table 11) for both Freundlich and Langmuir isotherms. The magnitudes of n , were close to unity resulting to $1/n$ that is above 1 for the adsorbates. Notably, despite the high R^2 values for SCP sorption onto Fe-MC, the plots yielded negative Langmuir isotherm constants (Q_0 and K_L).

Table 11: Calculated adsorption isotherm values

Isotherm model	SCP	SDM
Freundlich	$R^2=0.955$	$R^2=0.703$
	$n=0.939$	$n=0.970$
Langmuir	$k_f=0.293$ L/mg	$k_f=0.286$ L/mg
	$R^2=0.961$	$R^2=0.669$
	$Q_0=-2.915$ mg/g	$Q_0=-1.264$ mg/g
Temkin	$K_L=-9.110 \times 10^{-2}$ L/mg	$K_L=-0.185$ L/mg
	$R^2=0.960$	$R^2=0.794$
	$b_T=9.029$ kJ/mol	$b_T=9.914$ kJ/mol
	$A_T=2.290$ L/mg	$A_T=3.182$ L/mg

4.4.4 Binary solute sorption of SCP and SDM onto Fe-MC clay

The equilibrium experimental data for the simultaneous sorption of SCP onto Fe-MC in the presence of an equal concentration of SDM (1 mg L^{-1}) is shown in Table 12. The sorption of SCP was significantly reduced by the presence of SDM in the bi-component system. The equilibrium sorption capacity of SCP decreased from 0.362 mg/g in the single component solution to 0.226 mg/g in the binary solution (Table 12) with the value $R_{q,SCP} = 0.625$ being much less than 1. The equilibrium sorption capacity of SDM was 0.203 mg/g in single component solution and 0.2096 mg/g in binary solution, resulting to the value $R_{q,SDM} = 1.032$, almost equivalent to 1.

Table 12: Single and binary sorption of SCP and SDM onto Fe-MC

Sorption capacity (mg/g)	SCP	SDM
Single component ($q_{s,i}$)	0.362	0.203
Binary component ($q_{b,i}$)	0.226	0.209

4.5 Thermodynamics of SCP and SDM sorption onto untreated and Fe-MC clays

The effect of temperature was evaluated in the temperature range of 303 to 323 K. When the temperature was raised from 303 to 323 K, the amount of SCP and SDM adsorbed onto untreated clay after equilibrium decreased (Table 13). The thermodynamic parameters, namely, change in Gibbs free energy (ΔG), enthalpy (ΔH), entropy (ΔS) and activation energy (E_a) (Table 6), were derived from the van't Hoff and Henry's law equations defined earlier are then listed in Table 13.

Table 13. Thermodynamic parameters for SCP and SDM sorption onto raw clay

Compound	Temp (K)	Adsorption capacity (mg g ⁻¹)	ΔG (kJ mol ⁻¹)	ΔH (kJ mol ⁻¹)	ΔS (J mol ⁻¹)	E_a (kJ mol ⁻¹)	S^*
SCP	303	0.704	-17.839				
	313	0.693	-18.287	-2.551	50.39	0.771	0.517
	323	0.691	-18.849				
SDM	303	0.508	-15.738				
	313	0.506	-16.237	-3.259	41.27	1.636	0.267
	323	0.488	-16.559				

Both the enthalpy change (ΔH) and Gibbs free energy changes (ΔG) were negative for both SCP and SDM at all the temperatures examined. The entropy change (ΔS) values were positive while the magnitudes of the activation energies (ΔE_a) were typically below 5 kJ mol⁻¹.

Similarly, as in the raw clay, the amount of SCP and SDM adsorbed onto Fe-MC decreased with increase in temperature (Table 14). Negative values of enthalpy change (ΔH) and Gibbs free energy changes (ΔG) are also reported accompanied by positive entropy change (ΔS) values.

Table 14. Thermodynamic parameters for SCP and SDM sorption onto Fe-MC

Compound	Temp (K)	Adsorption capacity (mg/g)	ΔG (kJ/mol)	ΔH (kJ/mol)	ΔS (J/mol)	E_a (kJ/mol)	S^*
SCP	303	0.465	-15.302				
	313	0.444	-15.586	-7.562	25.570	4.219	0.0873
	323	0.419	-15.812				
SDM	303	0.362	-14.230				
	313	0.343	-14.487	-7.594	29.930	5.004	0.0498
	323	0.320	-14.667				

CHAPTER FIVE

5.0 DISCUSSION

The previous chapter outlined the results obtained for all experiments conducted. This chapter discusses at length the physical meaning and implications of the aforementioned findings.

5.1 Adsorbent characterization

5.1.1 Chemical composition

The elemental composition of oxide form of the raw (untreated) clay (RC) and iron modified treated clay (Fe-MC) obtained from XRF analyses as presented in Table 5 depict successful incorporation of iron in to the clay matrix. The raw clay contained oxides of various cations including Na, K, Mg, Ba, Ca and Zr and the relative variation in their percentages after chemical treatment indicate that iron modification possibly involved cation exchange or the iron oxide was precipitated onto the clay mineral surface replacing the elements previously observed on the raw clay mineral layer. As several authors (Gao et al., 2016; Goncalves et al., 2013; Hassan and Hameed et al., 2011) have observed, the lower than expected iron oxide content incorporated in the clay matrix could be due to iron leaching during synthesis by the wet impregnation method. A significant increase in Na content was realized.

5.1.2 Textural characteristics of the raw and Fe-MC clays

The textural characteristics (Table 6) indicated no change in the Brunauer–Emmett–Teller (BET) specific surface area of the Fe-MC showing minimal blockage of the raw clay pores by the iron oxide particles and any intercalation of the iron particles did not result in exfoliation of the layered structure. The pore volumes data calculations are consistent with this conclusion (Gao et al., 2016). The results indicate that a change in chemical composition does not necessarily affect textural characteristics and interlayer spacing.

5.1.3 Functional groups analysis

Apart from XRD, literature affirms FTIR spectroscopy as a magnificent tool for distinguishing and quantifying the different magnetic iron oxides, namely magnetite (Fe_3O_4) and maghemite ($\gamma\text{-Fe}_2\text{O}_3$) (Namduri and Nasrazadani, 2008). The structural features and functional groups present are displayed in the FTIR plot (Fig. 2). Generally, there was decrease in intensities of all the bands in the Fe-MC relative to those in raw clay with no observable new peak formation. The absorption

band at 3694 cm^{-1} corresponds to the structural interlayer surface -OH stretching vibration while a corresponding prominent band at 3619 cm^{-1} indicate the existence of outer -OH groups probably from surface adsorbed and interlayer water. The absorption band at 910 cm^{-1} was assigned to an -OH deformation vibration at the alumina (Al-OH) faces (Konan et al., 2009). The peak at 1635 cm^{-1} corresponded to H-O-H bending of interlayered water molecules. The relative reduction of the 1635 cm^{-1} peak in Fe-MC is due to loss of the loosely physisorbed water molecules by heating (Zhao et al., 2012). This loss of hydroxyl groups may reduce the sorption capacity of the clay for the target molecules. The band centered at 750 cm^{-1} corresponds to Si-O-Al vibrations (Hassan and Hameed et al., 2011). The characteristic absorption bands of the Fe-O bond in bulk magnetite (Fe_3O_4) appear at 570 cm^{-1} and 375 cm^{-1} (Namduri and Nasrazadani, 2008) while maghemite (Fe_2O_3) has several characteristic bands centered at 556 cm^{-1} , 638 cm^{-1} and 696 cm^{-1} (Ercuta et al., 2013). Therefore, the two bands located at 595 cm^{-1} and 684 cm^{-1} indicates the presence of maghemite ($\gamma\text{-Fe}_2\text{O}_3$) phase. Furthermore, when Fe_3O_4 is heated at low temperatures of about $200\text{-}250^\circ\text{C}$ in an oxidizing atmosphere, ($\gamma\text{-Fe}_2\text{O}_3$) is formed (Correa et al., 2006).

5.1.4 Crystallinity of raw and Fe-MC clays and structural changes analysis

Fig. 3 showed the XRD patterns of the raw clay and the Fe-MC sample. The dwarf diffraction peaks at $2\theta = 11.98^\circ$, 20.70° , 21.30° and 45.18° correspond to kaolinite while the sharp peaks at $2\theta = 26.48^\circ$, 31.52° and 42.28° , depict the other crystalline phase of the clay as quartz (Hassan and Hameed, 2011). The diffractions at $2\theta = 30.08^\circ$, 36.46° and 42.3° in Fe-MC are characteristic of $\gamma\text{-Fe}_2\text{O}_3$ evidencing presence of maghemite in the impregnated clay and corroborates the findings from FTIR data previously discussed. The slight but noticeable decrease in the intensity of the quartz peak at $2\theta = 26.48$ in Fe-MC suggests subtle changes in crystallinity of quartz due to thermal treatment (Shvarzman et al., 2003). Comparing the analogous peaks reveal increased disorder in Fe-MC than untreated clay. The interlayer space was 7.27\AA for both samples which is comparable to the molecular size dimensions of sulfonamides (Braschi et al., 2010) making adsorbate intercalation, within the interlayer spaces, possible.

5.2 Adsorption kinetics

5.2.1 Kinetics studies of SCP and SDM onto untreated clay

The time-dependent evolution of raw clay sorption capacity for SCP and SDM depicted fast sorption kinetics leading to saturation within 180 min (Fig. 4) followed by an equilibrium phase. The rapid initial sorption rate is due to availability of completely vacant active sorption sites followed by the slow equilibrium phase attributed to saturation of the energetically favourable surfaces. Noteworthy, kaolinite clay exhibited higher removal efficiency for SCP (77%) than SDM (50%).

The sorption dynamics were analyzed using linearized Lagergren pseudo-first order and pseudo-second order kinetic models. The conformity to the models was evaluated by the linear correlation coefficient (R^2) values and comparing the experimental equilibrium sorption density (q_{exp}) with the theoretical values (q_{cal}) computed from the kinetic model. The data poorly fitted the pseudo-first order model with low R^2 values. On the contrast, the data perfectly fitted the pseudo-second-order kinetics law with R^2 (>0.99) closest to unity (Fig. 5) corroborated with exact convergence of the calculated (q_{cal}) and experimental (q_{exp}) sorption capacities (Table 7). The half-life values indicate SCP sorption exhibited faster kinetics than SDM.

5.2.2 Kinetics studies of SCP and SDM onto Fe-MC clay

The variation of SCP and SDM retention by Fe-MC as a function of time depicted that the sorption extent of the compounds increased rapidly to saturation within 180 min (Fig. 7) followed by a stagnated phase with no appreciable changes, implying attainment of equilibrium conditions at this stage. The observed rapidity at the initial stages is due to a high solute concentration gradient and availability of completely bare active binding sites followed by the slow equilibrium phase attributed to saturation of the binding surfaces and repulsion between the adsorbed molecules and those in the bulk phase. Fe-MC exhibited higher removal efficiency for SCP (75%) than SDM (45%). Noteworthy, the raw clay had slightly higher removal efficiency than Fe-MC for both compounds. This is possibly due to loss of some of the $-OH$ groups as noted in the FTIR analysis above and some amorphous organic phase during thermal treatment that may aid in sorption.

The pseudo-first order likewise presented poor R^2 values. Therefore, it's implied that the mechanism of the sorption of SCP and SDM onto Fe-MC does not follow pseudo-first order

kinetics which assumes one adsorbate molecule is attached to one binding site. The pseudo-second-order rate law satisfactorily described the adsorption systems under study with R^2 (>0.99) closest to unity (Fig. 4) corroborated with the close agreement between the calculated (q_{cal}) and experimental (q_{exp}) adsorption capacities (Table 4) with less than 2% deviation. The pseudo-second order model assumes that one adsorbate molecule is sorbed onto two active sites of the Fe-MC clay. The half-life values indicate SCP sorption exhibited faster kinetics than SDM. The kinetic data was also fitted to the intra-particle diffusion model (Weber and Morris, 1963) to predict the rate-controlling step. According to the model, if the plot of q_t versus $t^{0.5}$ is linear, then pore diffusion occurs and if the plot passes through the origin, intra-particle diffusion is the only rate-controlling step. Positive C values depict boundary layer effects while negative C values denote no boundary layer effects on the adsorption rate (Elwakeel *et al.*, 2014). As observed in figure 8, the plots were multi-linear implying the sorption process occurred in phases and pore-diffusion was not the sole operating rate controlling step.

5.3 Adsorption isotherm studies

5.3.1 Single solute of SCP and SDM sorption onto raw clay

In the present work, equilibrium data modeling for single component system was done using three linearized isotherms *viz.* Langmuir, Freundlich and Temkin and their constants are listed in Table 4. From the Langmuir model, K_L is the Langmuir adsorption constant ($L\ mg^{-1}$) related to the free energy of adsorption and Q_o is the maximum monolayer adsorption density ($mg\ g^{-1}$) while for Freundlich model, K_f and n are Freundlich constants depictive of the relative adsorption capacity and adsorption favorability or surface heterogeneity of the adsorbent, respectively. According to Treybal (1981), the values of n in the range 2-10 represent good, 1-2 moderately difficult, and less than 1 a poor adsorptive property.

From the R^2 values, Langmuir model satisfactorily predicted the sorption of SCP while not perfectly, though fairly for SDM over the untreated clay. Kaolinite had a higher Langmuir maximum monolayer adsorption density for SCP than SDM (Table 9). The favorability of the adsorption process was obtained in terms of the dimensionless separation constant R_L given by equation 14.

Precisely, R_L values describe the nature of the adsorption process to be either unfavourable ($R_L > 1$), linear ($R_L = 0$), favourable ($0 < R_L < 1$) or irreversible ($R_L = 1$). The calculated R_L values in the

present work (Table 4) indicate the sorption processes are favourable. On the other hand, the magnitude of Freundlich constant n , lying between 1-2, indicate a moderately difficult adsorption process for both adsorbates while $1/n$ is between 0 and 1 indicating the heterogeneity of the sorption surfaces of the clay. Therefore, both models fairly represent the sorption of SCP and SDM onto the clay despite the variances in R^2 .

5.3.2 Binary solute sorption of SCP and SDM onto raw clay

The equilibrium experimental data for the simultaneous sorption of SCP onto raw clay in the presence of an equal concentration of SDM (1 mg L^{-1}) is shown in Table 10. Competitive sorption of SCP and SDM onto the raw clay in a binary solute system was evaluated by comparison of the ratio of the equilibrium sorption capacities (R_q), as defined by equation 10.

In this context, when $R_{q,i} > 1$, the presence of another adsorbate in a bi-component system appreciates the sorption of contaminant i (i.e., synergistic sorption), if $R_{q,i} = 1$, there is no effect of the simultaneous presence of the other adsorbate in the binary system on the sorption of compound i and if $R_{q,i} < 1$, the abstraction of compound i is significantly diminished by the presence of the competing adsorbate molecules (i.e., antagonistic sorption) (Istratie *et al.*, 2016).

Here, the sorption of SDM was significantly abridged by the presence of SCP in the binary system. The equilibrium sorption capacity of SDM decreased from 0.314 mg g^{-1} in the single solute solution to 0.142 mg g^{-1} in the binary solution (Table 10). The value $R_{q,SDM} = 0.453$ is far less than 1 confirming antagonistic sorption of SDM in the presence of SCM. By contrast, SCP sorption was practically unaffected by the presence of SDM in the binary system. The equilibrium sorption capacity of SCP was 0.353 mg g^{-1} in single solute solution and 0.323 mg g^{-1} in binary solution, resulting to the value $R_{q,SDM} = 0.915$, tending to 1.

Consequently, the decrease of SDM sorption in the presence of SCP ($R_{q,SCP} = 0.625$) while SCP sorption was almost constant ($R_{q,SCP} = 0.915$) indicate much stronger interactions between SCP and the untreated clay binding sites than those involved in SDM sorption. The results also suggest that SCP and SDM do not share some binding sites suggesting somewhat different sorption mechanisms are also involved.

5.3.3 Single solute of SCP and SDM sorption onto Fe-MC clay

Isothermal modeling are prerequisites for evaluating the distribution of the adsorbates between the aqueous and solid phases and the nature of the adsorbate-adsorbent interactions. In the present work, equilibrium data modeling for single component system was done using three widely used two-parameter isotherms *viz.* Langmuir, Temkin and Freundlich and their constants are listed in Table 11. Sorption of SDM onto Fe-MC showed low linearity posting relatively low coefficients of determination, R^2 , (Table 11) for both Freundlich and Langmuir isotherms. Moreover, the magnitudes of n , close to unity, indicate moderately difficult adsorptive process. Nevertheless, from the R^2 values only, both models could not adequately predict the sorption of SDM over Fe-MC suggesting multiple sorption mechanisms are involved. The hypothesized cooperative adsorption involving multiple mechanisms is also implied by the $1/n$ that is above unity for adsorbates (Saleh, 2015). Moreover, despite the high R^2 values for SCP sorption onto Fe-MC, the negative Langmuir isotherm constants (Q_o and K_L) values bore no physical meaning and are unacceptable. This depicts that the underlying assumptions of Langmuir modelization are incapable to satisfactorily explain the sorption of SDM and SCP onto Fe-MC and would yield dimensionless separation constant (R_L) value greater than 1 (Shikuku et al., 2015). These negative constants also impose a limitation on the use of the adsorption isotherm constants in determination of heats of adsorption. This may suggest a change in adsorption mechanism compared to sorption of SCP and SDM onto untreated kaolinite clay under similar conditions which conformed to linearized Langmuir equation. Alternatively, this observation may also be attributed to the inherent error structures associated with transformation of non-linear functions to linear models (Nagy et al., 2017). Linearization process can violate the theories underneath the model and the estimated parameters may not necessarily represent the same values for the original non-linear equation. To overcome this problem, the SCP and SDM equilibrium sorption data were fitted to the original non-linear Langmuir equation to ascertain that the sorption mechanisms are not governed by postulates of the Langmuir model as implied by the linear regression analysis.

Non-linear regression of equilibrium sorption data for each isotherm was performed by minimizing the regression sum of squares (RSS) error function using the *solver* add-in with excel's spreadsheet, Excel (Microsoft) and the calculated constants and the coefficients of determination are presented in Table 15 below. The RSS error function was obtained as the sum of the squares of the differences

between the experimental data and data values predicted by the models. Mathematically, this is represented as:

$$RSS = \sum_1^N (q_{e,experimental} - q_{e,predicted})^2 \quad (16)$$

Where N is the number of data points. In the non-linear analysis, there was significant variation in the Langmuir constants and R^2 values. From the R^2 values, the sorption of SCP was describable by the Langmuir model. Unlike in linear regression, all the constants were positive. The Langmuir monolayer maximum adsorption capacities were 4.561 and 1.789 mg/g for SCP and SDM, respectively. It is evident therefore that linearization contributed in the violation of the theoretical basis of the model. The results demonstrate that while linear regression is widely used to determine isotherm models of best fit; non-linear regression is a better analytical method to avoid errors in estimation of isotherm parameters and prediction of best fit models. There was no significant variation in the constants and R^2 values for the non-linear Freundlich and Temkin isotherms relative to linear analysis. Based on R^2 values, the best fitting model were in the order Temkin>Langmuir>Freundlich.

Table 15: Non-linear regression analysis for SCP and SDM sorption onto Fe-MC

	Langmuir coefficients			Freundlich coefficients			Temkin coefficients		
	Q_0 mg/g	K_L L/mg	R^2	n	K_f L/mg	R^2	b_T kJ/mol	A_T L/mg	R^2
SCP	4.561	0.069	0.997	0.977	0.293	0.953	9.029	2.924	0.998
SDM	1.789	0.193	0.756	1.162	0.289	0.748	9.878	3.175	0.794

5.3.4 Binary solute sorption of SCP and SDM onto Fe-MC clay

The equilibrium experimental data for the simultaneous sorption of SCP onto Fe-MC in the presence of an equal concentration of SDM (1 mg L^{-1}) is shown in Table 12. The parameter $R_{q,i}$ is as earlier explained in section 5.3.2. The sorption of SCP was significantly reduced by the presence of SDM in the bi-component system. The equilibrium adsorption capacity of SCP decreased from 0.362 mg/g in the single component solution to 0.226 mg/g in the binary solution (Fig 6).

The value $R_{q,SCP} = 0.625$ is much less than 1 confirming antagonistic sorption of SCP in the presence of SDM.

By contrast, SDM sorption was practically unaffected by the presence of SCP in the binary system. The equilibrium sorption capacity of SDM was 0.203 mg/g in single component solution and 0.2096 mg/g in binary solution, resulting to the value $R_{q,SDM} = 1.032$, almost equivalent to 1.

The observed decrease of SCP uptake in the presence of SDM ($R_{q,SCP} = 0.625$) while SDM sorption was kept variably constant ($R_{q,SDM} = 1.032$) imply much stronger interactions between SDM and the Fe-MC binding sites than those involved in SCP sorption. The results also indicate that SCP and SDM do not share some binding sites hence exhibit different sorption mechanisms.

The comparison between the adsorption capacities of the adsorbent reported in this work will selected materials tested for some sulfonamides is represented in Table 16. It can be seen that the adsorption capacities reported in the present work are comparable and would perform better under lower temperature conditions as those reported in literature due to the exothermic nature of the sorption processes as will be discussed in the next section.

Table 16: Comparison of adsorption capacities of selected adsorbents for sulfonamide compounds

Adsorbent	Adsorbate	Adsorption capacity (mg/g)	Temperature (K)	Reference
Hydrous ferric oxide	Sulfadimethoxine	1.123	288	Zhu et al., 2016
Hydrous ferric oxide	Sulfadimethoxine	1.298	298	Zhu et al., 2016
Hydrous ferric oxide	Sulfadimethoxine	1.401	308	Zhu et al., 2016
Activated carbon	Sulfamethazine	3.071	298	Liu et al., 2017
Fe-modified activated carbon	Sulfamethazine	17.241	298	Liu et al., 2017
Raw kalolinite clay	Sulfadimethoxine	1.391	303	This study
Fe-MC	Sulfadimethoxine	1.789	303	This study
Raw kalolinite clay	Sulfachloropyridazine	8.547	303	This study
Fe-MC	Sulfachloropyridazine	4.561	303	This study

5.4 Thermodynamics of SCP and SDM sorption onto raw and Fe-MC clays

Generally, temperature changes have two diverse effects on an adsorption process: under pre-equilibrium conditions it alters the rate of adsorption while after the equilibrium attainment; temperature changes alter the position of adsorption equilibrium of the adsorbent for a given adsorbate.

When the temperature was raised from 303 to 323 K, the amount of SCP and SDM adsorbed onto both raw clay and Fe-MC after equilibrium decreased (Table 13 and 14) depicting an exothermic sorption process. This is attributable to increased molecular solubility with rise in temperature hence decreased affinity for the adsorbent surface with concomitant weakening of the adsorbate-kaolinite forces and increased molecular mobility hence the molecules escape from the adsorbent surfaces into the liquid phase. The decrease in amount adsorbed denotes the shifting of the equilibrium toward desorption with rise in temperature. The thermodynamic parameters, namely, changes in free energy (ΔG), entropy (ΔS) and enthalpy (ΔH), which indicate the practical feasibility of the process, post-adsorption structural changes of the adsorbent and the adsorption mechanism, respectively, derived from the van't Hoff and Henry's law equations are given in Table 13 and 14.

The negative values of enthalpy change (ΔH) affirm the exothermic nature of the sorption reactions. The observed consistent decrease in adsorption capacity (q_e), mg/g, with rise in temperature (Table 6) denotes a shift of the equilibrium position to reverse direction of the reaction. Moreover, magnitudes of ΔH below 40 kJ mol^{-1} depict physisorption mechanisms (Saleh, 2015). In this study, the computed ΔH values (Table 13 and 14) indicate that physisorption is the dominant sorption mechanism of both SCP and SDM onto both untreated and untreated clay. Also, ΔG values for physisorption range between 0 and 20 kJ mol^{-1} while those for chemisorptions are between 80 and 400 kJ mol^{-1} (Atkins, 1990). Thus, the magnitudes of the ΔG values reported in this work also attest to the physical nature of the sorption process of both compounds on both adsorbents. The negative ΔG for both SCP and SDM, at all temperatures, indicate the sorption processes onto kaolinite were thermodynamically spontaneous and favorable. The positive values of entropy change (ΔS) correspond to an increase in molecular disorderliness at the solid/liquid interface of the adsorption a testament that the sorption phenomenon is enthalpically driven and not enthalpy-governed. To further ascertain that physisorption is the predominant adsorption mechanism, the sorption

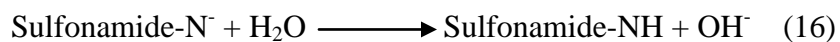
activation energy (E_a) and sticking probability (S^*) were computed from experimental data following modified Arrhenius type equation (equation 8) connected to surface coverage (θ) expressed by equation 9 (Mahoud et al., 2016). The magnitude of activation energy gives further insight on whether the sorption involves a physical or chemical process. Generally, physisorption processes have energies in the range of 5–40 kJ/mol, while higher activation energies (40–800 kJ mol⁻¹) point to a chemisorption mechanism (Atkin, 1990). The E_a values for the sorption of SCP and SDM onto the untreated and Fe-MC clays were in the range 4-5 kJ mol⁻¹, strengthening the aforementioned hypothesis of physisorption being the sorption mechanism. These values also indicate the existence of a low potential energy barrier.

5.5 Adsorption mechanism of SCP and SDM onto raw and Fe-MC clays

In order to understand the sorption mechanisms and the adsorbates-adsorbent interactions, the surface charge, functional groups present and composition of the adsorbent relative to the physico-chemical properties of SCP and SDM were studied. Several possible sorption mechanisms reported for sulfonamides were considered, namely: (1) hydrophobic partitioning; (2) electrostatic attraction; (3) cation bridging; and (4) negative charge-assisted H-bond [(-) CAHB] (Teixido et al., 2011). The higher removal efficiency for SCP ($\log K_{ow}$ 0.31) than SDM ($\log K_{ow}$ 1.17) depicted that other mechanisms besides hydrophobic interaction were involved in sorption process. Furthermore, changes from neutral to anionic form increase the hydrophilicity of the sulfonamides and thus hydrophobic interactions become significantly lessened (Ma et al., 2012). Electrostatic interactions are known to influence sorption of ionic compounds. In the present study, SCP and SDM molecules ($pK_a = 5.7$) were mostly anionic under the circumneutral experimental conditions (pH of 6.4). The pH of point of zero charge (pH_{pzc}) of both untreated and Fe-MC clays, which is an index of the clay mineral layer (surface) charge as a function of pH, was about 6.1 (Fig. 1) and therefore the net surface charge of the adsorbent was negative at pH above this value. This testifies that the sorption of SCP and SDM onto the clays could not be attributed to coulombic attractions.

From XRF analysis, the clays contained several multivalent cations (M^{n+}) (Table 5). These multivalent cations may promote adsorption of the negatively charged species (SCP⁻ and SDM⁻) by surface bridging with these anions. Therefore, the adsorption of SCP and SDM may be partly attributed to cation bridging interactions. Such clay-adsorbate interactions may be correlated with

the molecular dipole moment (Debye). The most polar sulphonamide (SCP) (Table 1) was adsorbed more. This suggests that the adsorption variance of SCP and SDM between the untreated clay and Fe-MC clay as depicted in the kinetic and isothermal studies is closely linked to their polarity. Furthermore, the similarity in the pK_a values (5.7) and the pH_{pzc} (6.1) makes it conceivable that strong (-)CAHB forms between the anionic SCP/SDM species and the negatively charged clay surfaces. Furthermore, the similarity in the pK_a values (5.7) and the pH_{pzc} (6.2) makes it conceivable that strong (-)CAHB forms between the anionic SCP/SDM species and the Fe-MC surface hydroxyl groups. This would involve proton exchange with water molecules as shown in equation 14 releasing $-OH$ into the solution. The $-OH$ would then be neutralized by deprotonation of the Fe-MC surface hydroxyl groups by formation of negative charge-assisted H-bond [(-) CAHB] (equation 15) as schematically presented in Fig. 9.



Similar affinity between molecules with comparable pK_a to surface hydroxyl groups have been reported for sorption of sulfamethoxazole (SMX) and sulfamethazine (SMZ) on biochars (Lian et al., 2014; Ma et al., 2012). Iron leaching into the solution from the adsorbent matrix was monitored using AAS and was below the instrumental LOQ (0.01 mg L^{-1}).

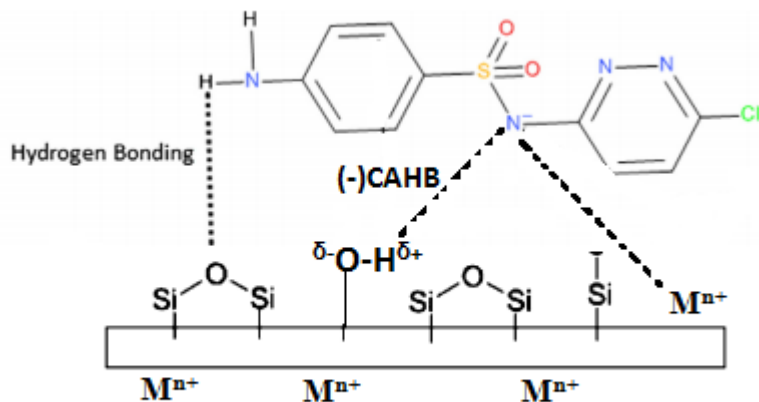


Figure 9: Possible adsorption mechanism of SCP on raw clay and Fe-MC

5.6 Batch adsorption reaction design

According to Omri et al. (2016), adsorption isotherms can be used predict the design of batch adsorption regimes. The aim of the design is to predict the mass of raw clay, m (g), required to remove sulfonamide solution of volume V (L), from a near real environmental initial concentration of C_o to relatively permissible levels of concentration C_e (mg L^{-1}) for a single solute sorption system.

Since the isothermal studies indicated that the Langmuir isotherm model satisfactorily described the equilibrium sorption data for SCP and SDM onto the untreated clay, the mass of untreated clay, m (g), required to achieve a certain percentage removal efficacy (R) from aqueous solution of volume V (L) for a pre-determined initial concentration of sulfonamide C_o (mg L^{-1}), excluding 100% removal efficiency was calculated by the relation:

$$m = \frac{VRC_o(1 + K_L(C_o(1 - R/100)))}{100Q_oK_L(C_o(1 - R/100))} \quad (17)$$

Fig. 10 and 11 below shows plots of computed mass of raw clay and Fe-MC, respectively, required for removing SCP and SDM from aqueous media simulating real environmental reported initial concentration of 0.2 mg L^{-1} to achieve 99% removal efficiency for solutions of varied volumes (1-10 L) at 303 K for a single-component batch reactor. Despite the expected increase in the amount of adsorbent required with increase in the volume of effluent to be cleaned, the fact that approximately 0.8 kg, obtained from equation 18, is required to eliminate 99% of 0.2 mg L^{-1} both sulfonamides in 10 L solution attest to the sustainability of the clay as a low-cost adsorbent.

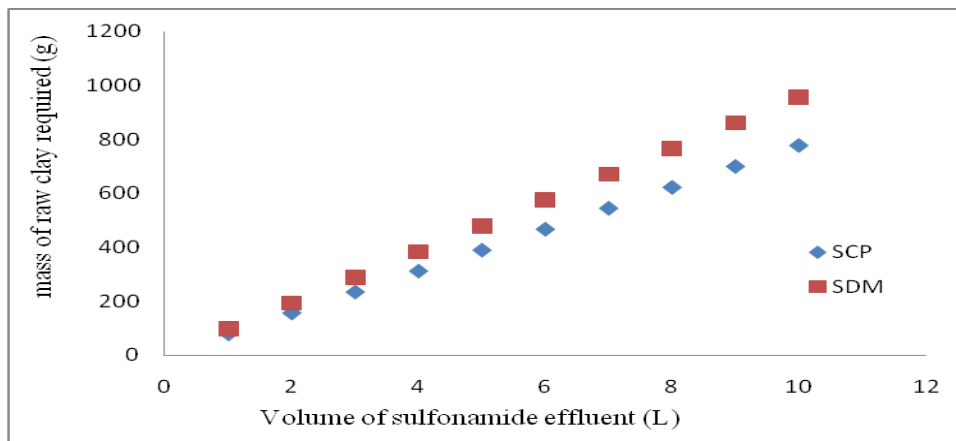


Figure 10: Theoretical variation of mass of untreated clay required with volume for SCP and SDM effluents to be treated for 99% sorption efficiency with initial concentration of 0.2 mg L^{-1} at 303 K

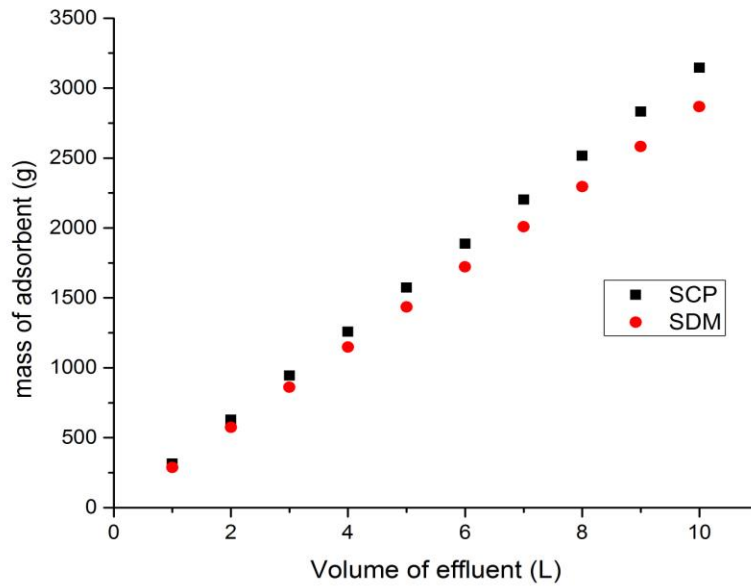


Figure 11: Variation of the theoretical mass of Fe-MC with volume required for SCP and SDM effluents to be treated for 99 % removal efficiency with initial concentration of 0.2 mg L^{-1} at 303K

CHAPTER SIX

CONCLUSION AND RECOMENDATIONS

6.1 Conclusion

1. The untreated clay samples were mainly composed of kaolinite and quartz as the main crystalline phases.
2. Iron oxide in form of maghemite was successfully incorporated into the clay matrix through in lower than expected amounts. The surface of morphology of the Fe-MC clay was different from the raw clay besides differences in chemical composition. The chemical treatment did not affect the interlayer spacing and surface area.
3. The Langmuir best described the sorption of SCP and SDM onto the raw and Fe-MC clays. For the raw clay, the maximum monolayer adsorption densities were 8.547 and 1.391 mg g⁻¹ for SCP and SDM, respectively. For Fe-MC, the Langmuir monolayer maximum adsorption capacities were 4.561 and 1.789 mg/g for SCP and SDM, respectively. SCP sorption was higher than SDM for each adsorbent
4. In binary solute solutions, an antagonistic sorption process of SDM ($R_{q,SCP}= 0.453$) in the presence of SCP ($R_{q,SDM}=0.915$) was observed for the untreated clay suggesting replacement sorption. However, for the Fe-MC clay, the binary sorption study showed an antagonistic sorption process of SCP ($R_{q,SCP}= 0.625$) in the presence of SDM ($R_{q,SDM}=1.032$), an opposite phenomenon to the observation for the untreated clay.
5. The sorption capacities were found to be unfavored by rise in temperature. The computed thermodynamic parameters, ΔG , ΔH , ΔS indicate that sorption of SCP and SDM onto both untreated and treated clays is spontaneous, exothermic and feasible. The Arrhenius activation energy (E_a) values (below 5 kJ mol⁻¹) depicted the sorption reactions to be physical in nature.
6. The sorption kinetics data followed the pseudo-second order kinetic law for both SCP and SDM onto the clay sorbents. The sorption half life was calculated and the sorption rate of SDM was faster (1.179 min) than that of SCP (3.873 min) onto the raw clay. On the contrary, the sorption rate of SCP (1.186 min) was faster than that of SDM (6.637 min) onto

the Fe-MC clay. Intraparticle diffusion model showed that the sorption of SCP and SDM onto the clay was multi-phased and pore diffusion was not the sole rate determining step.

7. It is realized that the sorption mechanism most likely involves cation bridging and negative charge-assisted H-bonding and is possibly controlled by the polarity of SCP and SDM molecules.

6.2 Recommendations

The raw clay was found to be a better adsorbent for SCP and SDM removal than Fe-MC clay despite Fe-MC having a slightly higher sorption capacity for SDM and can therefore be used in its untreated form. Linearization of adsorption isotherms is demonstrated to be an unsuitable analytical tool for predicting adsorption isotherms.

6.3 Suggestion for further research

Studies should be conducted to determine:

1. The most suitable method for incorporation of magnetic iron to the clay matrix to improve on adsorbent recovery step.
2. Desorption studies to evaluate the number of cycles the kaolinite clay may be used before losing its adsorptive potential
3. The efficacy of other clay minerals in removal of sulfonamides and other pharmaceutically active ingredients from water at near real environmental concentrations
4. Other suitable low cost and sustainable adsorbents for sulfonamides removal from water

REFERENCES

- Al-Rifai, J.H., Khabbaz, H., Schäfer, A.I. 2011. Removal of pharmaceuticals and endocrine disrupting compounds in a water recycling process using reverse osmosis systems. *Sep. Purif. Technol.* 77, 60-67.
- Attia, T.M.S., Hu, X.L., Qiang, Y.D. 2013. Synthesized magnetic nanoparticles coated zeolite for the adsorption of pharmaceutical compounds from aqueous solution using batch and column studies. *Chemosphere*, 93: 2076-2085.
- Baran, W., Adamek E., Justyna Z., Andrzej, S. 2011. Effects of the presence of sulfonamides in the environment and their influence on human health. *J. Hazard. Mater.* 1–15, 30 196.
- Basile, T., Petrella, A., Petrella, M., Boghetich, G., Petruzzelli, V., Colasuonno, S., Petruzzelli, D. 2011. Review of endocrine-disrupting compound removal technologies in water and wastewater treatment plants: An EU Perspective. *Ind. Eng. Chem. Res.* 50(14): 8389-8401.
- Białk-bielińska, A., Stolte, S., Arning, J., Uebers, U., Bösch, A., Stepnowski, P., Matzke, M. 2011. Ecotoxicity evaluation of selected sulfonamides. *Chemosphere*, 85, 928–933
- Boruah, P.K., Borah, D.J., Handique, J., Sharma, P., Sengupta, P., Das, M.R. 2015. Facile synthesis and characterization of Fe₃O₄ nanopowder and Fe₃O₄/reduced graphene oxide nanocomposite for methyl blue adsorption: A comparative study. *J. Environ. Chem. Eng.* 3, 1974–1985
- Braschi, I., Blasioli, S., Gigli, Lara., Gessa, C.E., Alberto, A., Martucci, A. 2010. Removal of sulfonamide antibiotics from water: Evidence of adsorption into an organophilic zeolite Y by its structural modifications. *J. Hazard. Mater.* 178, 218–225
- Chang, J., Jianchao, M., Qingliang, M., Duoduo, Z., Nannan, Q., Mengxiao, H. & Hongzhu, M. 2016. Adsorption of methylene blue onto Fe₃O₄/activated montmorillonite nanocomposite. *Appl. Clay Sci.* 119, 132–140
- Christen, V., Hickmann, S., Rechenberg, B., Fent, K. 2010. Highly active human pharmaceuticals in aquatic systems: A concept for their identification based on their mode of action. *J. Aquat. Toxicol.* 96, 167–181.
- Coey, J.M.D. 2009. Magnetism and magnetic materials. New York, NY: Cambridge University Press.
- Correa, J.R., Canetti, D., Castillo, R., Llopiz, J.C., Dufour, J. 2006. Influence of the precipitation pH of magnetite in the oxidation process to maghemite. *Mater. Res. Bull.* 41, 703–713
- Cottet, L., Almeida, C.A.P., Naidek, N., Viante, M.F., Lopes, M.C., Debacher, N.A. 2014. Adsorption characteristics of montmorillonite clay modified with iron oxide with respect to methylene blue in aqueous media. *Appl. Clay Sci.* 95, 25–31

- Daneshvar, A., Aboulfadl, K., Viglino, L., Broséus, R., Sauvé, S., Madoux-Humery, A., Weyhenmeyer, A., Prévost, M. 2012. Evaluating pharmaceuticals and caffeine as indicators of fecal contamination in drinking water sources of the Greater Montreal region. *Chemosphere*, 88, 131-139.
- Debrassi, A., Baccarin, T., Demarchi, C.A., Nedelko, N., Slawska-Waniewska, A., Dhuzewski, P., Bilska, M., & Rodrigues, C.A. 2012. Adsorption of Remazol Red198 onto magnetic N-lauryl chitosan particles: equilibrium, kinetics, reuse and factorial design. *Environ. Sci. Pollut. Res.* 19, 1594–1604.
- Dhruv, M., Siddharth, M., & Singha, S.K. 2015. Magnetic adsorbents for the treatment of water/wastewater—A review. *J. Water Process Eng.* 7, 244–265
- Ercuta, A., Chirita, M. 2013. Highly crystalline porous magnetite and vacancy-ordered maghemite microcrystals of rhombohedral habit. *J. Cryst. Growth* 380, 182–186
- Faulconer, E.K., Hoogesteijn von Reitzenstein, N.V. & Mazyck, D.W. 2012. Optimization of magnetic powdered activated carbon for aqueous Hg(II) removal and magnetic recovery. *J. Hazard. Mater.* 9–14.
- Freundlich, H.M.F. 1906. Ueber die adsorption in lösungen, *Z. Phys. Chem.* 57, 385–470.
- Fungaro, A., Yamaura, M., & Carvalho, T.E.M. 2011. Adsorption of anionic dyes from aqueous solution on zeolite from fly ash-iron oxide magnetic nanocomposite. *J. At. Mol. Sci.* 2 (4), 305–316
- Gao, Y., Guo, Y., Zhang, H. 2016. Iron modified bentonite: Enhanced adsorption performance for organic pollutant and its regeneration by heterogeneous visible lightphoto-Fenton process at circumneutral pH. *J. Hazard. Mater.* 302, 105–113
- Genc, N., Dogan, C. E. 2015. Adsorption kinetics of the antibiotic ciprofloxacin on bentonite, activated carbon, zeolite, and pumice. *J. Desalin. Water Treat.* 53(3): 785-793
- Ghosh, S., Badruddoza, A.Z., Hidajat, K. & Uddin, M.S. 2013. Adsorptive removal of emerging contaminants from water using superparamagnetic Fe₃O₄ nanoparticles bearing aminated-cyclodextrin. *J. Environ. Chem. Eng.* 122–130.
- Girginova, P.I., Daniel-da-Silva, A.L., Lopes, C.B., Figueira, P., Otero, M. & Amaral, V.S. 2010. Silica coated magnetite particles for magnetic removal of Hg²⁺ from water. *J. Colloid Interface Sci.* 234–240

- Gonçalves, M., Guerreiro, M.C., Oliveira, L. C., Soares, C. 2013. A friendly environmental material: Iron oxide dispersed over activated carbon from coffee husk for organic pollutants removal. *J. Environ. Manag.* 127, 206-211
- Hay, 1873. Patent No. 140. USA.
- Ho, Y. S. 2006. Review of second-order models for adsorption systems. *J. Hazard. Mater.* 136, 681-689.
- Ho, Y.S., McKay, G. 1998. Sorption of dye from aqueous solution by peat. *Chem. Eng. J.* 70, 115–124.
- Hollender, J., Zimmermann, S.G., Koepke, S., Krauss, M., McArdell, C.S., Ort, C., Singer, H., von Gunten, U., Siegrist, H. 2009. Elimination of organic micropollutants in a municipal wastewater treatment plant upgraded with a full-scale post-ozonation followed by sand filtration. *Environ. Sci. Technol.* 43(20): 7862-7869.
- Hosseinzadeh, H., Mohammadi, S. 2015. Quince seed mucilage magnetic nanocomposites as novel bioadsorbents for efficient removal of cationic dyes from aqueous solutions. *Carbohydr. Polymers* 134, 213–221
- Istratie, R., Marcela, S., Cornelia, P., Cosmin, L. 2016. Single and simultaneous adsorption of methyl orange and phenol onto magnetic iron oxide/carbon nanocomposites. *Arab. J. Chem.* <http://dx.doi.org/10.1016/j.arabjc.2015.12.012>
- Kara, Ali., Emel, D., Nalan, T., Bilgen, O., & Irli, N. 2015. Magnetic vinylphenyl boronic acid microparticles for Cr(VI) adsorption: Kinetic, isotherm and thermodynamic studies *J. Hazard. Mater.* 286, 612–623
- Kimosop, S.J., Getenga, Z.M., Orata, F.O., Okello, V.A., Cheruiyot, J.K. 2016. Residue levels and discharge loads of antibiotics in wastewater treatment plants and hospital lagoons within Lake Victoria Basin, Kenya. *J. Environ. Monit. Assess.* 188:532. DOI: 10.1007/s10661-016-5534-6
- Kolpin, D. W. Furlong, E.T, Meyer, M.T., Thurman, E.M., Zaugg, S.D., Barber, L.B., Buxton, H.T. 2002. Pharmaceuticals, hormones, and other organic wastewater contaminants in U.S. streams, 1999-2000: a national reconnaissance. *Environ. Sci. Technol.* 36, 1202–1211
- Koreje, K.O., Demeestere, K., De Wispelaere, P., Vergeynst, L., Dewulf, J., Langenhove, V. H. 2012. From Multi-residue Screening to Target Analysis of Pharmaceuticals in Water: Development of a New Approach Based on Magnetic Sector Mass Spectrometry and Application in the Nairobi River Basin. *Sci. Total Environ.* 437, 153-64.
- Kümmerer, K. 2009. Antibiotics in the aquatic environment—a review Part I. *Chemosphere*, 75, 417–434.

- Lakshmi, L., Das, N. 2013. Removal of caffeine from industrial wastewater using *Trichosporon asahii*. *J. Environ. Biol.* 34, 701-708.
- Langmuir, I. 1916. The constitution and fundamental properties of solids and liquids. *J. Am. Chem. Soc.* 38, 2221–2295.
- Le-Minh, N., Khan, S.J., Drewes, J.E., Stuetz, R.M. 2010. Fate of antibiotics during municipal water recycling treatment processes. *Water Res.* 44, 4296
- Li, X. M., Xu, G., Liu, Y., He, T. 2011. Magnetic Fe₃O₄ nanoparticles: Synthesis and application in water treatment. *Nanosci. Nanotechnol.* 1, 14-24
- Li, X., Qi, Y., Li, Y., Zhang, Y., He, X., Wang, Y. 2013. Novel magnetic beads based on sodium alginate gel crosslinked by zirconium(IV) and their effective removal for Pb²⁺ in aqueous solutions by using a batch and continuous systems. *Bioresour. Technol.* 611–619.
- Lian, F., Sun, B., Song, Z., Zhu, L., Qi, X., Xing, B. 2014. Physicochemical properties of herb-residue biochar and its sorption to ionizable antibiotic sulfamethoxazole. *Chem. Eng. J.* 248, 128–134
- Lisouza, F.A., Owuor, P.O., Lalah, J.O. 2011. Variation in indoor levels of polycyclic aromatic hydrocarbons from burning various biomass types in the traditional grass-roofed households in Western Kenya. *J. Environ. Pollut.* 159: 1810-1815.
- Liu, Y., Chen, M., Hao, Y. 2013. Study on the adsorption of Cu(II) by EDTA functionalized Fe₃O₄ magnetic nanoparticles. *Chem. Eng. J.* 46–54.
- Liu, Y., Liu, X., Dong, W., Zang, L., Kong, Q., Wang, W. (2017). Efficient adsorption of Sulfamethazone onto modified activated carbon: A plausible adsorption mechanism. *Sci. Rep.* 7, 12437
- Lu, A., H, Salabas, E. L., Schuth, F. 2007. Magnetic Nanoparticles: Synthesis, protection, functionalization and application (Review). *Angewandte chemie international edition in English*, 46, 1222-1244
- Ma, J., Jia, Y., Jing, Y., Yao, Y., Sun, J. 2012. Kinetics and thermodynamics of methylene blue adsorption by cobalt–hectorite composite. *Dyes Pigm.* 93, 1441–1446.
- Ma, Y., Li, M., Wu, M., Li, Z., Liu, X. 2015. Occurrences and regional distributions of 20 antibiotics in water bodies during groundwater recharge. *Sci. Total Environ.* 518–519, 498–506
- Mahmoodi, N.M. 2013. Magnetic ferrite nanoparticle–alginate composite: synthesis, characterization and binary system dye removal. *J. Taiwan Inst. Chem. Eng.* 44, 322–330

- Mahmoud, H.R., Ibrahim, S.M., El-Molla, S.A. 2016. Textile dye removal from aqueous solutions using cheap MgO nanomaterials: Adsorption kinetics, isotherm studies and thermodynamics. *Adv. Powder Technol.* **27**, 223–231
- Mayo, J.T., Yavuz, C., Yean, S., Cong, L., Shipley, H., Yu, W., Falkner, J., Kan, A., Tomson, M. & Colvin, V.L. 2007. The effect of nanocrystalline magnetite size on arsenic removal. *Sci. Technol. Adv. Mater.* **8** (1-2), 71-75.
- Mehta, D., Mazumdar, S., Singh, S.K.. Magnetic adsorbents for the treatment of water/wastewater- A review. *J. Water Process. Eng.* **7** (2015) 244–265
- Mestre, S.A., Bexiga, A.S., Proen, M., Andrade, M., Pinto, M.L., Matos, I., Fonseca, I.M., Carvalho, A.P. 2011. Activated carbons from sisal waste by chemical activation with K₂CO₃: Kinetic of paracetamol and ibuprofen removal from aqueous solution. *Bioresour. Technol.* **102**, 8253-8260.
- Michael, I., Rizzo, L., McArdell, C.S., Manaia, C.M., Merlin, C., Schwartz, T., Dagot, C., Fatta-Kassinos, D. 2013. Urban wastewater treatment plants as hotspots for the release of antibiotics in the environment: A review. *Water Res.* **47**, 957–995.
- Miège, C., Choubert, J.M., Ribeiro, L., Eusèbe, M., Coquery, M. 2009. Fate of pharmaceuticals and personal care products in wastewater treatment plants - Conception of a database and first results. *Environ. Pollut.* **157**(5), 1721-1726.
- Ngeno, E., Orata, F., Lilechi, D.B, Shikuku, V.O., Kimosop, S. 2016. Adsorption of caffeine and ciprofloxacin onto pyrolytically derived water hyacinth biochar: Isothermal, kinetics and thermodynamics. *J. Chem.Chem. Eng.* **10**, 185-194.
- Ngumba, E., Gachanja, A., Tuhkanen, T. 2016. Occurrence of Selected Antibiotics and Antiretroviral Drugs in Nairobi River Basin. *Sci. Total Environ.* **539**, 206-213.
- Oller, I., Malato, S., Sanchez, Perez, J. A., 2011. Combination of advanced oxidation processes and biological treatments for wastewater decontamination. A review. *Sci. Total Environ.* **409** (20), 4141-4166.
- Orata, F., Quinete, N. and Wilken, R. (2009). Long chain perfluorinated alkyl acids derivatisation and identification in biota and abiota matrices using gas chromatography. *Bul. Environ. Contam. Toxicol.* **83**, 630-35.

- Parham, H., Zargar, B. & Shiralipour, R. 2012. Fast and efficient removal of mercury from water samples using magnetic iron oxide nanoparticles modified with 2-mercaptobenzothiazole. *J. Hazard. Mater.* 94–100.
- Peng, X., Xu, F., Zhang, W., Wang, J., Zeng, C. & Niu, M. (2014). Magnetic Fe₃O₄@silica xanthan gum composites for aqueous removal and recovery of Pb²⁺. *Colloids Surf. A Physicochem. Eng. Aspects*, 27–36.
- Phillips, P.J., Smith, S.G., Kolpin, D.W., Zaugg, S.D., Buxton, H.T., Furlong, E.T. 2010. Pharmaceutical formulation facilities as sources of opioids and other pharmaceuticals to wastewater treatment plant effluents. *Environ. Sci. Technol.* 44: 4910–6.
- Primel, E., Caldas, S., Escarrone, A. 2012. Multi-residue analytical methods for the determination of pesticides and PPCPs in water by LC-MS/MS: a review. *Open Chem.* 10, 876–899
- Ruiz, B., Cabrita, I., Mestre, A.S., Parra, J.B., Pires, J., Carvalho, A.P., Ania, C.O. 2010. Surface heterogeneity effects of activated carbons on the kinetics of paracetamol removal from aqueous solution. *Appl. Surface Sci.* 256, 5171-5175.
- Salem, T. M., Hu, X. L., Yin, D. Q. 2013. Synthesized magnetic nanoparticles coated zeolite for the adsorption of pharmaceutical compounds from aqueous solution using batch and column studies. *Chemosphere* 93, 2076–2085
- Sharma, Y.C., Srivastava, V., Singh, V.K., Kaul, S.N. & Weng, C.H. 2009. Nano-adsorbents for the removal of metallic pollutants from water and wastewater. *Environ. Technol.* 30 (6), 583-609.
- Shengsen, W., Bin, G., Yuncong, L., Anne, E., & Feng, H. 2016. Adsorptive removal of arsenate from aqueous solutions by biochar supported zero-valent iron nanocomposite: Batch and continuous flow tests. *J. Hazard. Mater.* <http://dx.doi.org/10.1016/j.jhazmat.2016.01.052>
- Shikuku, V. O., Donato, F. F., Kowenje, C. O, Zanella, R., Prestes, D.O, 2015. A comparison of Adsorption Equilibrium, Kinetics and Thermodynamics of Aqueous phase Clomazone between Faujasite X and a Natural zeolite from Kenya. *S. Afr. J. Chem.* 68, 245-252.
- Singer, A.C., Nunn, M.A., Gould, E.A., Johnson, A. C. 2007. Potential risks associated with the proposed widespread use of Tamiflu. *Environ. Health Perspect.* 115 (1), 102–106.
- Singh, K.P., Gupta, S., Singh, A.K., & Sinha, S. 2011. Optimizing adsorption of crystal violet dye from water by magnetic nanocomposite using response surface modeling approach. *J. Hazard. Mater.* 186, 1462–1473.

- Stackelberg, P.E., Furlong, E.T., Meyer, M.T., Zaugg, S.D., Henderson, A.K., Reissman, D.B. 2004. Persistence of Pharmaceutical compounds and other organic Waste water contaminants in a convectional drinking water treatment plants. *Sci. Total Environ.* 329: 99-113.
- Straub, J. O. 2009. An environmental risk assessment for oseltamivir (Tamiflu (R)) for sewage works and surface waters under seasonal-influenza- and pandemic-use conditions. *Ecotoxicol. Environ. Safety.* 72 (6), 1625-1634.
- Tania, D. (Ed), 2012. *Nanotechnology for Water Purification*. Florida: Brown Walker Press.
- Teixeira, M.R., Rosa, S.M., Sousa, V. 2011. Natural organic matter and disinfection by-products formation potential in water treatment. *Water Resour. Manage.* 25(12), 3005-3015.
- Tireli, A.A., Francielle, C.F., Laís, F.O., Iara, R.G., Mário, C.G., Joaquim P.S. 2014. Influence of magnetic field on the adsorption of organic compound by clays modified with iron. *Appl. Clay Sci.* 97–98, 1–7
- Treybal, R.E. 1981. *Mass-transfer Operations*, 3rd ed., McGraw-Hill.
- Von Gunten, U. 2003. Ozonation of drinking water: Part I. Oxidation kinetics and product formation. *Water Res.* 37(7), 1443-1467.
- Wu, D., Zheng, P., Chang, P.R., & Ma, X. 2011. Preparation and characterization of magnetic rectorite/iron oxide nanocomposites and its application for the removal of the dyes. *Chem. Eng. J.* 174, 489–494.
- Wu, Q., Feng, C., Wang, C., Wang, Z. 2013. A facile one-pot solvothermal method to produce superparamagnetic graphene–Fe₃O₄ nanocomposite and its application in the removal of dye from aqueous solution. *Colloids Surf. B: Biointerf.* 101, 210–214.
- Xiaolei, Q., Pedro, J.J., Qilin, L. 2013. Applications of nanotechnology in water and wastewater treatment. *Water Res.* 47, 3931-3946
- Xing, M., Lejin, X., Jianlong, W. 2016. Mechanism of Co(II) adsorption by zero valent iron/graphene nanocomposite. *Journal of Hazardous Materials* 301, 286–296
- Yan, H., Li, H., Yang, H., Li, A., Cheng, R. 2013. Removal of various cationic dyes from aqueous solutions using a kind of fully biodegradable magnetic composite microsphere. *Chem. Eng. J.* 223, 402–411.

- Yang, X., Flowers, R.C., Weinberg, H.S., Singer, P.C. 2011. Occurrence and removal of pharmaceuticals and personal care products (PPCPs) in an advanced wastewater reclamation plant. *Water Res.* 45(16), 5218-5228.
- Yao, Y., Miao, S., Liu, S., Ma, L.P., Sun, H., Wang, S. 2012. Synthesis, characterization, and adsorption properties of magnetic Fe₃O₄@graphene nanocomposite. *Chem. Eng. J.* 184, 326–332.
- Yu, J.X., Wang, L.Y., Chi, R.A., Zhang, Y.F., Xu, Z.G., Guo, J. 2013. Competitive adsorption of Pb²⁺ and Cd²⁺ on magnetic modified sugarcane bagasse prepared by two simple steps. *Appl. Surf. Sci.* 163–170.
- Zhang, G., Qu, J., Liu, H., Cooper, A.T., Wu, R. 2007. CuFe₂O₄/activated carbon composite: a novel magnetic adsorbent for the removal of acid orange II and catalytic regeneration. *Chemosphere*, 1058–1066.
- Zhang, Q., Jia, A., Wan, Y., Hu, J. 2014. Occurrences of Three Classes of Antibiotics in a Natural River Basin: Association with Antibiotic-Resistant Escherichia coli. *Environ. Sci. Technol.* 48, 14317–14325
- Zhang, X., Zhang, P., Wu, Z., Zhang, L., Zeng, G., Zhou, C. 2013. Adsorption of methylene blue onto humic acid-coated Fe₃O₄ nanoparticles. *Colloids Surf. A Physicochem. Eng. Aspects*, 85–90
- Zhang, Z. and Kong, J. 2011. Novel magnetic Fe₃O₄@C nanoparticles as adsorbents for removal of organic dyes from aqueous solution. *J. Hazard. Mater.* 193, 325–329.
- Zhao, F., Zhang, B., Feng, L. 2012. Preparation and magnetic properties of magnetite nanoparticles. *Mater. Lett.* 68, 112–114
- Zhu, W., Wang, J., Wang, Y., Wang, H. 2016. Study on Sulfadimethoxine removal from aqueous solutions by ferric oxides. *Water Sci. Technol.* 74(5), 1136-1142